N-acetylation of secreted proteins in Apicomplexa is widespread and is independent of the ER acetyl-CoA transporter AT1

Mary Akinyi Nyonda, Jean-Baptiste Boyer, Lucid Belmudes, Aarti Krishnan, Paco Pino, Yohann Couté, Mathieu Brochet, Thierry Meinnel, Dominique Soldati-Favre, Carmela Giglione

N-Acetylation of secreted proteins is widespread in Apicomplexa and independent of acetyl-CoA ER-transporter AT1

Mary Akinyi Nyonda[1], Jean-Baptiste Boyer[2], Lucid Belmudes[3], Aarti Krishnan[1], Paco Pino[1,4], Yohann Couté[3], Mathieu Brochet[1], Thierry Meinnel[2,*], Dominique Soldati-Favre[1,*], Carmela Giglione[2,*]

[1]Department of Microbiology and Molecular Medicine, University of Geneva, Geneva, Switzerland
[2]Université Paris-Saclay, CEA, CNRS, Institute for Intergrative Biology of the Cell (I2BC), 91198 Gif-sur-Yvette, France
[3]Université Grenoble Alpes, INSERM, CEA, UMR BioSanté U1292, CNRS, CEA, FR2048, 38000 Grenoble, France.
[4]ExcellGene SA, CH1870 Monthey, Switzerland

*Authors for correspondence**:** (carmela.giglione@i2bc.paris-saclay.fr; dominique.soldati-favre@unige.ch; thierry.meinnel@i2bc.paris-saclay.fr).

Keywords: *Toxoplasma gondii, Plasmodium berghei*, Acetyl-CoA transporter, Acetylation, Secretory pathway, Endoplasmic Reticulum

ABSTRACT

Acetyl-CoA participates in post-translational modification of proteins, central carbon and lipid metabolism in several cell compartments. In mammals, the acetyl-CoA transporter 1 (AT1) facilitates the flux of cytosolic acetyl-CoA into the endoplasmic reticulum (ER), enabling the acetylation of proteins of the secretory pathway, in concert with dedicated acetyltransferases including NAT8. However, the implication of the ER acetyl-CoA pool in acetylation of ER-transiting proteins in Apicomplexa is unknown. We identify homologues of AT1 and NAT8 in *Toxoplasma gondii* and *Plasmodium berghei*. Proteome-wide analyses revealed widespread N-terminal acetylation marks of secreted proteins in both parasites. Such acetylation profile of

N-terminally processed proteins was never observed so far in any other organisms. *AT1* deletion resulted in a considerable reduction of parasite fitness. In *P. berghei*, AT1 is important for growth of asexual blood stages and production of female gametocytes and male gametocytogenesis impaling its requirement for transmission. In the absence of AT1, the lysine and N-terminal acetylation sites remained globally unaltered, suggesting an uncoupling between the role of AT1 in development and active acetylation occurring along the secretory pathway.

Summary statement

The apicomplexan acetyl-CoA transporter is indispensable for parasite development and transmission. This role is unrelated to the extensive acetylation of secreted proteins which apicomplexans display.

INTRODUCTION

Plasmodium species and *Toxoplasma gondii* are obligate intracellular parasites, members of the phylum of Apicomplexa and of clinical relevance, causing malaria and toxoplasmosis, respectively. In the search for newer, safer and more efficient drugs or vaccines and given the continuous emergence of resistance to available drugs, there is an urgent need for the identification of novel cellular targets for intervention.

Acetyl-CoA is a membrane impermeable metabolite made up of an acetyl (CH_3CO) group joined to Coenzyme A (CoA), which plays a central role in protein modification as well as lipid and central carbon metabolism and a promising target for antimalarials (de Vries et al., 2021). In both *T. gondii* and *Plasmodium spp*., acetyl-CoA is produced in the mitochondrion atypically through branched-chain α-keto acid dehydrogenase-complex (BCKDH), which uses pyruvate as a substrate. In the apicoplast, a relict plastid organelle derived from secondary endosymbiosis, pyruvate is converted to acetyl-CoA by the pyruvate dehydrogenase complex (PDH) (Fleige et al., 2007, Cobbold et al., 2013), while in the nucleo-cytosol compartment of *T. gondii,* two routes of production are implemented, through acetyl-CoA synthetase (ACS) from acetate and ATP citrate lyase (ACL) from citrate (Tymoshenko et al., 2015). In contrast, cytosolic acetyl-CoA is only produced through ACS in *Plasmodium*

falciparum (Cobbold et al., 2013). In-depth analysis of the contribution of these distinct acetyl-CoA pools to parasite physiology revealed that abrogation of production of cytosolic acetyl-CoA in the cytosol of *T. gondii* led to inhibition of fatty acid elongation, reduced lysine (K)-acetylation of 115 proteins in both secretory and nucleo-cytosolic compartments and ultimately led to parasite death (Kloehn et al., 2020). Indeed, acetyl-CoA is also used by specific enzymes (N-terminal-α-acetyltransferases, NATs, and lysine acetyltransferases, KATs) to modify by acetylation the N-termini or the side chains of lysines of proteins (Friedmann & Marmorstein, 2013; Montgomery *et al*, 2015; Drazic *et al*, 2016). Accordingly, to the substrate specificity, different NATs have been characterized. In brief, NatA corresponds to the complex involved in N-terminal acetylation (NTA) of proteins which first methionine has been cleaved, NatB/C/E modify proteins with N-terminal methionines, while NatD and NatH are specific for NTA of histone and actin isoforms, respectively (Aksnes et al., 2019).

. Acetylation on both N-termini and side chains of lysine residues of proteins have been reported in both pathogens with over one thousand proteins in *P. falciparum* (Cobbold et al., 2016). Exported proteins including red blood cell surface directed proteins have their signal peptides and host-targeting motifs cleaved by an endopeptidase Plasmepsin V in the parasite ER (Boddey et al., 2010, Russo et al., 2010, Osborne et al., 2010). An acetyl moiety is then transferred from acetyl-CoA to the newly formed N-termini catalyzed by a specific but uncharacterized ER-resident acetyl-CoA acetyltransferase priming proteins for trafficking (Chang et al., 2008, Osborne et al., 2010). In *T. gondii* tachyzoites, trafficking of the majority of rhoptry and microneme proteins to their respective secretory organelles occurs through the ER and Golgi. Rhoptry discharge requires proteolytic maturation of proteins at the N-termini by aspartyl protease (ASP3) present at a post Golgi location termed as the endosome-like compartment (ELC) (Dogga et al., 2017). Furthermore, a subset of GRAs undergo proteolytic cleavage by ASP5 at the Golgi (Hammoudi et al., 2015, Coffey et al., 2018).

In mammalian cells, acetyl-CoA is actively translocated into the ER lumen via an acetyl-CoA transporter (AT1), a polytopic membrane protein belonging to a family of symporters localized in the ER membrane (Jonas et al., 2010). AT1 mediated import of acetyl-CoA into the ER facilitates acetylation of lysine residues on proteins by resident NAT8 acetyltransferases (Jonas et al., 2010, Pehar and Puglielli, 2013,

Dieterich et al., 2019, Farrugia and Puglielli, 2018). Homologues of AT1 can be found in model organisms including *Saccharomyces cerevisiae, Caenorhabditis elegans* and *Drosophila melanogaster* (Hirabayashi et al., 2004) but not in the plastid-containing *Arabidopsis thaliana* plant model. A putative AT1 homologue has also been localized to the ER both in *P. falciparum* (Lim et al., 2016) and *T. gondii* (Tymoshenko et al., 2015, Barylyuk et al., 2020). However, the importance of acetyl-CoA import into the ER and its role in post-translational acetylation of secreted proteins have not been investigated to date. Genome wide fitness screens have revealed that *P. berghei* AT1 (Pb*AT1*) contributes to blood stage forms development (Bushell et al., 2017) and is essential for transmission to mosquitoes (Stanway et al., 2019). In contrast *T. gondii* AT1 (Tg*AT1*) has a fitness score of -0.07 according to the CRISPR-Cas9 screen, suggesting that it may be dispensable during the tachyzoite stage in tissue culture (Sidik et al., 2016).

In this study, we performed an N-terminomics analysis of *T. gondii* and *P. berghei*. This unveiled the occurrence of a dedicated N-terminal protein processing machinery featuring proteolysis followed by acetylation in several compartments within apicomplexan parasites, including the secretory pathway. Such frequent N-terminal acetylation of proteins of the secretory pathway was never described so far in another organism. Together, the data indicate the existence in these parasites of N-acyltransferases exhibiting substrate specificity comparable to that observed for NatA, B, C, D, E and H. Accordingly, homologs of several cytosolic Nat catalytic subunits could be retrieved in the proteomes of *T. gondii* and *P. berghei.* A NAT8 homolog is so far the only likely candidate for ER-located protein acetylation and it is essential for parasite growth. Likewise, AT1 is the only candidate to fuel the ER acetylation pathway, independently of the acetyltransferase activity involved. The gene encoding for AT1 was deleted in *P. berghei* and *T. gondii*, respectively, resulting in considerable reduction of parasite fitness. Unexpectedly, global acetylome profiling of both N-α-termini and ε-lysine in both *T. gondii* and *P. berghei* AT1-KOs reveals modest or no alteration of the acetylomes of secretory proteins. Overall, this study highlights the role of AT1 in parasite fitness and specifically in gametogenesis in *P. berghei*. This role is however not correlated with the protein acetylation of ER-transiting proteins and suggests a bypass alternative route

ensuring acetyl-CoA import occurring along the secretory pathway in the absence of AT1.

RESULTS

N-terminomics analysis unveils the existence of a typical N-terminal protein processing machinery in Apicomplexa

The role of acetyl-CoA in the secretion pathway of apicomplexan parasites is poorly understood. We searched for signs of its existence through protein modifications on acceptor amino groups (i.e., N-α and N-ε groups). Widespread N-ε-lysine-acetylation (K-acetylation) of proteins has been observed in various compartments of *T. gondii* RH parasites, including the ER (Kloehn et al., 2020, Jeffers and Sullivan, 2012, Xue et al., 2013). In contrast, only a handful of studies is currently available on the maturation of proteins via their N-terminus and the machinery involved in apicomplexan parasites (Dogga et al., 2017, Chang et al., 2008). N-terminal acetylation (NTA) profiles allow not only relative but also absolute quantitative measurements, with stoichiometric assessment of the acetylation yield (i.e., [% acetylated]/[% acetylated+non-acetylated]). To further get into the protein acetylome of these parasites, we performed a global NTA quantitative analysis on both parasites using the SILProNAQ procedure as described previously (Frottin et al., 2016, Bienvenut et al., 2015). The complete unfiltered data search yielded 169 and 181 non-redundant N-termini for *P. berghei* and *T. gondii,* respectively (Table S1, S2 and Fig. S1A). The corresponding proteins arose from several compartments including mostly the cytosol, the nucleus, mitochondria, ER and the post-Golgi secretory pathway (rhoptries, micronemes, dense granules etc, Sheiner and Soldati-Favre, 2008). The associated functions deal with protein synthesis, proteostasis (chaperones/proteolytic), cytoskeleton (actin/myosins), glycolysis, Krebs cycle and DNA-binding proteins including histones and the specific apicomplexan machinery (see protein description, Gene Ontology and subcellular location annotations in sheets 4 of Tables S1 and S2). The data showed that N-terminal Methionine Excision (NME) occurs in apicomplexans with a specificity similar to that reported in other eukaryotes (Fig. 1A). NME is slightly more frequent in *T. gondii* than in *P. berghei* (Fig. 1A), probably determined by their respective codon usage. In contrast,

the frequency of NTA was found to be lower in *T. gondii* compared to *P. berghei* (67% vs 82%) (Table S1 and S2). However, NTA is associated with similar specificities in both organisms (Fig. 1B), with Met, Ser and Ala N-termini being almost systematically N-α acetylated (NTAed) (Tables S1 and S2 sheets 5). In addition, quantitative analysis showed that NTAed proteins have high average acetylation yields of 96±1 and 92±1 in *P. berghei* and *T. gondii*, respectively. NTA in apicomplexan parasites follows the rules of acetylation identified in other eukaryotes with substrates mostly arising from the activity of the major enzymatic complexes. This involves the NatA complex specific for NME-induced N-termini, and NatB, NatC and NatE, which modify proteins retaining an N-terminal Met (Fig. 1C). Furthermore, N-terminal acetylation of histones H2A/B suggests the existence of an active NatD in *T. gondii*. The identification of NTAed actin peptides (DEEVQALVVD) witnesses NatH unique activity on N-terminal acidic residues (see TGME49_209030 in Table S1, sheet 3). In *P. berghei*, the actin N-terminus was retrieved (GDEEVQALVI) which does not appear to result from NatH but rather from NatA acetylation (PBANKA_1459300 in Table S2, sheet 3). We noticed that NatA activity is favored in *T. gondii*, similar to other eukaryotes (Fig. 1C, Fig. S1A and Table S1 Sheet 6). In *P. berghei*, an unprecedented preference for NatB activity was noted, unique to our knowledge and in agreement with a reduced NME process in this organism (Fig. 1C, Fig. S1A and Table S2). Our data also indicate that the N-termini of proteins of all major compartments of the parasites except the apicoplast could be identified. NTA is similar in all compartments retrieved including ER- and post-Golgi-located proteins of the secretory pathway (Table S3). Interestingly, *T. gondii* showed an unusually high level of NTAed proteins belonging to the secretory pathway.

We compared this newly generated *T. gondii* dataset with reanalyzed and unfiltered data from previous publications (Dogga et al., 2017, Coffey et al., 2018). The analysis revealed a strong correlation of changes on the N-termini amongst all three datasets (Table S1). Compilation of all these datasets brought 696 non-redundant proteoforms with at least one N-terminal acetylated peptide with the following characteristics: 159 N-termini start at the first Met and 318 at the second amino acid. The NME rules imposed by methionine aminopeptidases specificity are identical to those observed in other organisms (Martinez et al., 2008, Frottin et al., 2009, Frottin et al., 2016). Filtering out downstream N-termini starting with a Met or having a Met

at position -1, we additionally retrieved 87 N-termini (Table S1) accurately matching the NME rules and thus strongly corresponding to the proper translation start and allowing to re-annotate the N-terminus of those proteins. Among the retrieved N-termini starting at position 1 or 2, we observed N-terminal acetylation of 161 N-termini for which we could quantify the yield of NTA in 88 of them (Table S1).

Interestingly, the analysis of the N-terminal acetylated peptides in the enlarged compiled dataset (Table S1) further confirms the existence of *T. gondii* N-acyltransferases showing substrate specificity comparable to that observed for NatA, B, C and E in other organisms (Aksnes et al., 2016, Giglione and Meinnel, 2021). Similar results were obtained when we applied the SILProNAQ pipeline to *P. berghei* extracts (Table S2 and Fig. S1A). Accordingly, homologs of the NatA/B/C/D/E/F catalytic subunits NAA10/20/30/40/50/60 could be retrieved in the proteome of *T. gondii* (Table S4). Homologs of only NAA10/20/30/40 were identified in *P. berghei,* while NAA50 and NAA60 were missing as also appears to be the case in other Plasmodium species including *P. falciparum* (Rathore et al., 2016) (Table S4). Finally, we could identify a homolog of the auxiliary NAA15 subunit of the NatA complex in Apicomplexa but failed to identify the auxiliary subunit HypK (Table S4). We identified a homolog of the auxiliary subunit NAA25 of NatB in *T. gondii* but not in *Plasmodium spp* (Table S4). As NAA25 was shown to be required for NatB activity in yeast and mammal cells (Van Damme et al., 2012), the absence of identification of a clear NAA25 sequence homolog in Plasmodium *spp* might mean that the catalytic subunit of these organisms evolved to ensure the NatB function alone or another non-sequence homolog protein ensures the auxiliary function. Additionally, as for NatB, we did not identify either the NAA35 nor the NAA38 subunits, the auxiliary subunits of NatC, in both *T. gondii* and *P. berghei.* NatH (NAA80) homologs could not be retrieved either in apicomplexan parasites. Nevertheless, such activity does exist in *T. gondii* as discussed before. Finally, the identified apicomplexan Nat catalytic subunit domains showed strong similarities to those of all other eukaryotes including human with the exception of NAA30 (Fig. S2).

N-terminal acetylation of new N-termini originating from proteolytic cleavage along the secretory pathway in parasites

As reported above, our *T. gondii* N-terminal acetylome data features a high percentage of NTAed proteins. 23% (42 entries; Fig.1A) displayed an N-terminal

starting well beyond the second amino acid. 14 of them displayed acetylation with yield >20%. From this list, we realized that 10 out the 42 needed to be discarded as they start with a Met or on a residue which is preceded by a Met, which fits with NME rules (see also above). Within the list of the NTAed peptides starting downstream of position 2, we identified six proteins in the secretory pathway (GRA1, GRA2, GRA7, GRA9, ROP9, SRS30C) for which NTA yield was always higher than 95%, when measurable. When the same filtering was applied to the qualitative and published N-acetylomes (Dogga et al., 2017, Coffey et al., 2015) completed with our current quantitative data, 94 proteins displayed both starts much beyond the N-terminal Met and with doubtless NTA status (Table S1 and Fig. S1A). 31 of them - including some GRAs, MICs, RONs, ROPs, SRSs, aminopeptidase N and aspartyl protease ASP5 - are well-recognized to be associated to the secretory pathway and to undergo signal peptide and/or further proteolytic processing. We noticed that several of these proteins display multiple cleavage sites either within vicinal residues next to a main proteolytic cleavage site or much beyond with NTA associated at each site compiled (Table S1 and Fig. S1A). This implies that NTA may occur all along the secretory pathway at the ER and results from several independent proteolytic cleavages starting with signal peptide removal (Fig. S1B). As proteolytic processing of these proteins was already described to occur in the ER, we concluded that an NTA machinery is likely associated with the ER. Substrate specificity of this NAT appears similar to that of a NatA, as it modifies mostly small residues like A, G, S, T or V. The associated number of such proteins is as high as for cytosolic proteins. Yet, unusual N-terminal residues including L, K and H were retrieved to undergo NTA, but for none of them quantification was possible, preventing a conclusion about the efficiency of this NTA. This unusual substrate specificity is very similar to that of plastid GNATs (pGNAT) of plants, working on plastid-imported proteins after the cleavage of the transit peptide (Giglione and Meinnel, 2021, Bienvenut et al., 2020). However, no such pGNAT homolog could be retrieved in apicomplexan proteomes. The low frequency of processed proteins in *P. berghei* (3 proteins) did not allow us concluding whether *Plasmodium* spp. do also display such machinery. We cannot exclude that ER NTA is associated to later differentiated states of the parasite or to different interactions with the host.

Together, the data suggest the occurrence of an N-terminal machinery located in the ER of apicomplexan parasites, with specificity corresponding mainly to a NatA, but also broader including NatB as the retrieved amino acids were A>>G, M, S, T or V.

T. gondii encodes multiple acetyltransferases that distribute to various sub-cellular compartments

The above data suggest NTA activity in several compartments within apicomplexan parasites. Using sequences of known eukaryotic N-terminal acetyltransferases (NATs), the GCN5--related *N*-acetyltransferases family, we performed genome searches in ToxoDB.org and PlasmoDB.org and obtained 15 putative acetyltransferase enzymes in *T. gondii* as reported before (Cova et al., 2018), 7 out of 15 matching the human NAT enzymes already characterized (Table S4). In addition, we examined the prediction of contribution of each putative enzyme to the fitness of parasites as follows: *T. gondii* tachyzoites based on CRISPR-Cas9 genome-wide screen (Sidik et al., 2016), blood stage of *P. berghei* based on detection of barcoded mutants (Bushell et al., 2017) and transposon mutagenesis in *P. falciparum* blood stages (Zhang et al., 2018) (Table S4). The subcellular localization of some of these proteins are predicted by hyperLOPIT results (Table S4) (Barylyuk et al., 2020).

Because of their unusual primary structure featuring long N-terminal extensions before the C-terminal acetyltransferase predicted domain which could influence their subcellular localization and drive them to the ER, we focused on three *T. gondii* genes encoding homologues of the conserved GNAT machinery for further investigations of the ER acetylation machinery (Fig. S3A): TGME49_259070 encoding the putative catalytic NAA30 subunit of NatC (named TgNAA30), TGME49_305450 encoding a putative NAT8 enzyme, an ER-resident protein N-acetyltransferase (Ko and Puglielli, 2009, Mak et al., 2014), named TgNAT8, and TGME49_221160 encoding a putative NAT with no known homologues, (named TgNAT) (Table S4, Fig. S3A). The three selected putative NATs are predicted to contribute to tachyzoite stage fitness based on their negative fitness scores (TgNAA30 -2.51, TgNAT -1.69, TgNAT8 -1.32) and all proteins bear the conserved catalytic acetyltransferase GNAT domain (Fig. S3B). TgNAT8 is predicted to occupy similar subcellular localization as its human homologue, while localization information is missing for TgNAT and TgNAA30 (Table S4). TgNAT8 is conserved in

all apicomplexans, whereas TgNAA30 is present in Coccidia and Haemosporidia and TgNAT is coccidian specific (Fig. S3A). We identified the NTAed terminus of TgNAT8 located on Alanine 2 (Table S1, sheet 4) which is compatible with its expression in Toxoplasma with a cytosolic N-terminal side and the GNAT domain within the ER guided by the unique TM-domain (Fig. S3B).

To study the function of these three enzymes, protein degradation elements, mini auxin induced degron (mAID) coupled to 3-Ty epitope tags (2885 nucleotides), were fused at the C-termini of TgNAT8 and TgNAA30 in parasites expressing the plant auxin (IAA) reporter TIR1 (Brown et al., 2018) (Fig. S3C). Several attempts at fusing the mAID-3Ty construct at the C-terminus of TgNAT were unsuccessful, plausibly due to its bulk, hence a smaller DiCre driven U1 pre-mRNA degradation sequence fused to 3-Ty epitope tags, (2473 nucleotides) were inserted at the C-terminus in the endogenous locus (Pieperhoff et al., 2015) (Fig. S3D). These strategies allowed the localization as well as the conditional depletion of the proteins upon addition of IAA or rapamycin. Localization of the putative NAT and TgNAT8 was established through immunofluorescence assay. NAA30mAID-Ty exhibited a granulated cytosolic appearance, matching the cytosolic localization of its homologues (Fig. 2A). NAT8mAID-Ty exhibited a perinuclear, residual body and cytosol presence which is representative of the parasite ER localization (Fig. 2A). NAT-U1-DiCre-Ty was confined to the parasite nucleus and colocalized with the nuclear DNA marker DAPI (Fig. 2A). Addition of IAA led to downregulation of the targeted proteins. Western blots of extracellular parasites with or without treatment showed NAA30mAID-Ty and NAT8mAID-Ty to migrate between the 70 and 100 kDa, their predicted molecular weights are 52 and 57 kDa, respectively, with subsequent protein loss upon treatment with IAA (Fig. 2B). Down-regulation of NAA30 did not affect parasite development, assessed by plaque formation seven days post infection of confluent human foreskin fibroblast (HFFs), ($p=0.2619$, -Auxin) and ($p=0.9911$, +Auxin) (Fig. 2C and 2D). Examination of the intracellular growth of parasites treated or not with IAA for 24 hours showed that, downregulation of NAA30 did not influence parasites replication (Fig. 2E). Depletion of TgNAT8 on presence of auxin led to a minor but non-significant impact in intracellular growth (Fig. 2E). Concordantly, slight change in plaque formation were observed upon treatment of NAT8mAiD parasites ($p=0.3187$, -Auxin) and ($p=0.0593$, +Auxin) (Fig. 2C and D).

AT1 is conserved in apicomplexan parasites

Among all identified candidates, the NAT8 homologue TgNAT8 might display physiological function compatible with protein acetylation in the ER, when taking in account its localization and parasite fitness. In addition, although NAT8 was so far shown to acetylate lysine side chains, it is not excluded that this protein, as the recent plastid GNATs, might display dual KA and NTA activities. Because modification of the ER localized TgNAT8 induced drastic parasite development defects, we surmised that perturbation of any member of the ER acetylation machinery, particularly ER-AT1 might dramatically affect ER protein acetylation. As NATs and NAT8 rely on Acetyl-CoA, we challenged the origin of this compound in the ER. Mammalian AT1 translocates acetyl-CoA into ER lumen (Jonas et al., 2010) while *Plasmodium* and *T. gondii* have an intricate acetyl-CoA synthesis and utilization network (Fig. 3A). Therefore, we investigated the impact of deletion of the ER-acetyl-CoA transporter AT1 on parasite fitness and its link to ER protein acetylation.

Mammalian AT1 sequences are highly similar, the human AT1 is predicted to contain a leucine zipper motif and multiple transmembrane domains (Hirabayashi et al., 2013). AT1 is present in Coccidia, Haemosporidia and Cryptosporidia but appears to be missing in Chromerida, Gregarina and Piroplasmida (Fig. 3B). *T. gondii* encodes only one putative TgAT1 (*TGGT1_215940*). TgAT1 localization to the ER was predicted through hyperplexed Localisation of Organelle Proteins by Isotopic Tagging (hyperLOPIT) and confirmed by epitope tagging (Barylyuk et al., 2020, Tymoshenko et al., 2015) (Fig. 3B). The protein contains 605 amino acids with 9 predicted transmembrane domains (TMDs) and a signal peptide at the N-terminus (Fig. 3C). PbAT1 is encoded by *PBANKA_0519800* and shares 30.5% amino acid identity with TgAT1 (Fig. S4A). PbAT1 is expressed in both erythrocytic asexual and sexual stages and with a peak of expression at the schizont stage (Fig. S4B and S4C). The protein contains 557 amino acids with 12 predicted TMDs and a coiled coil domain (Fig. 3B). PbAT1 and TgAT1 bear little similarity with the human AT1 sequence, 28.9% and 31.1%, respectively (Fig. S4A), which maybe be reflection of divergent evolution with an unknown bearing on functional roles.

AT1 is important for erythrocytic proliferation in *P. berghei*

In a large-scale signature tagged mutagenesis study, deletion of Pb*AT1* was reported to reduce growth of the asexual blood stage (Bushell et al., 2017, Stanway et al., 2019). To further investigate the requirements for PbAT1 in erythrocytic proliferation and in the *Plasmodium* life cycle (Fig. S4C and S4D), its encoding gene was deleted using the PlasmoGEM knock-out vector PbGEM_265292 (Fig. S4E and S4F) in the 820cl1mfcl1 clone to produce 820cl1Pb*AT1-KO*, to facilitate the phenotyping of sexual stages (Fig. S4G). This line expresses the green fluorescent protein (GFP) and the red fluorescent protein (RFP) under the control of a male and of a female-specific promoter, respectively (Mair et al., 2010). An independent Pb*AT1-KO* clonal line was generated in the 2.34 parental strain to produce 2.34Pb*AT1-KO* (Fig. S4G), and used for phenotyping Pb*AT1* deletion by immunofluorescence.

820cl1Pb*AT1-KO* showed a 14-fold reduction (p=0.0002) of parasitemia compared to the 820cl1mfcl1 mother line 6 days after the intraperitoneal injection of approximately 50,000 parasites (Fig. 3E). To confirm this severe growth phenotype, we investigated the relative growth of 820cl1Pb*AT1-KO* compared with the 2.34 parental line in a competition assay where a 5:1 820cl1Pb*AT1-KO*:WT ratio of parasites were simultaneously injected. The kinetics of 820cl1Pb*AT1-KO* and 2.34 parasite growths were measured over 6 days by flow cytometry where 820cl1Pb*AT1-KO* parasites were detected by the expression of GFP and RFP, while 2.34 parasites were detected by Hoechst staining. The 820cl1Pb*AT1-KO* line was out-competed by 2.34 parasites in less than 5 days post infection (Fig. 3F). Proliferation of asexual blood stages involves the invasion of new red blood cells (RBCs) by the merozoite forms upon rupture of infected RBCs by mature schizonts (Fig. 3D). Following a 16h *in vitro* culture, 820cl1Pb*AT1-KO* ring and trophozoite stages formed microscopically normal schizonts with a number of merozoites comparable to those of 820cl1mfcl1 parasites (p=0.6068) (Fig. 3G). To test whether the resulting merozoites were infective, blood containing approximately 50,000 820cl1Pb*AT1-KO* and 820cl1mfcl1 schizonts were injected intra-venously in naïve mice, respectively, and the ring parasitemia was determined 1h post injection by blood smear followed by microscopy. A similar number of circulating ring forms were detected in the 820cl1Pb*AT1-KO* and control groups (p=0.1695) (Fig. 3H). Presently, unavailability of a continuous culture system for *P. berghei* asexual blood stages limits the dissection of the entire RBC cycle *in*

vitro. Furthermore, examining these steps *in vivo* is technically challenging. Despite this, we have validated the findings that PbAT1 is crucial for proliferation *in vivo*.

PbAT1 is essential for the sexual development of *P. berghei*

Pb*AT1* was previously predicted to be essential for the parasite transmission to the mosquito (Stanway et al., 2019) (Fig. S4D). Transmission of *Plasmodium* parasites to the mosquito initially relies on an irreversible pre-commitment of a few asexual stage parasites into female gametocytes (macrogametocytes) or male gametocytes (microgametocytes). As gametocytes of both sexes mature, they dramatically reduce their metabolic activity and become quiescent, waiting for uptake into the mosquito during a blood feed to resume their development. In 820cl1Pb*AT1-KO* parasites, an average of 0.6% male gametocytemia compared to 1.32% was observed on day 3 following infection. Nearly no macrogametocytes could be detected in 820cl1Pb*AT1-KO,* with an average of 0.07% compared to 1.71% in wildtype parasites, resulting in an altered sex ratio (Fig. 4A). The male gametocyte of 820cl1Pb*AT1-KO* also appeared as empty and morphologically different from the wildtype ones through Giemsa staining (Fig. 4B). The findings therefore point to a role of PbAT1 during gametocytogenesis or sex determination.

We then investigated whether Pb*AT1-KO* microgametocytes were further able to form microgametes. Shortly after ingestion by a mosquito, microgametocytes undergo rapid gametogenesis at a permissive temperature in presence of xanthurenic acid, a small molecule present in the mosquito midgut (Billker et al., 1998). In about ten minutes, the haploid male gametocyte completes three rounds of genome replication and closed endomitosis, assembles the component parts of eight axonemes, and following nuclear division, produces eight flagellated motile male gametes in a process called exflagellation. Ten minutes post-activation, only 30% of the 820cl1Pb*AT1-KO* microgametocytes had attained octoploid status compared to 90% of the wildtype group. 40% of the 820cl1Pb*AT1-KO* microgametocytes remained haploid despite activation, while the remaining 20% and 10% attained diploid and tetraploid status respectively (Fig. 4C). Subsequent investigations post-activation of 2.34Pb*AT1-KO* microgametocytes by immunofluorescence imaging also revealed a defect in axoneme assembly and the absence of egress from the RBCs (Fig. 4D and 4E). As a result, no active exflagellation centers were formed by 2.34Pb*AT1-KO* microgametocytes p=0.0041 (Fig. 4F). Altogether, these findings

implicate that PbAT1 plays a critical function in female- and male gametocytogenesis associated with defective microgametogenesis in *P. berghei.*

TgAT1 is important for the lytic stages of *T. gondii*

To delete *TgAT1,* CRISPR-Cas9 mediated gene replacement with a drug selection cassette approach was used (Fig. S4H) and transfectants identified by genomic PCR (Fig. S4I). In *T. gondii*, AT1 was deleted in the RH strain (Tg*AT1-KO)* and shown to exhibit a significant defect in the lytic cycle development assessed seven days post infection *in vitro* by plaque size measurements on human foreskin fibroblast (HFFs), compared to the wildtype ($p<0.0001$) (Fig. 5A and 5B). This defect in growth was confirmed through growth competition assays (Fig. 5C). Tg*AT1-KO* parasites also displayed a slower intracellular development (Fig. 5D), but invasion of host cells was not impaired ($p=0.7207$) (Fig. 5E). These findings were unexpected, given the fitness score of -0.07, which indicates dispensability.

AT1 driven influx of acetyl-CoA into ER of apicomplexan parasites does not impact N-terminal acetylation of *T. gondii* proteins

As all known NATs use acetyl-CoA as sole acetyl donor, it is expected that dramatic acetyl-CoA depletion resulting from *at1* knockout might lead to decrease of the NTA of such proteins. We, therefore, performed comparative N-terminomics analysis on Tg*AT1-KO* and wild-type parasites. The complete unfiltered data yielded 1499 identified N-termini (793 in the combined wildtype and 706 in the mutant samples), including 200 non-redundant proteoforms (181 in wildtype and 143 in Tg*AT1-KO*). Out of this dataset, 140 unique N-termini were properly quantified (Fig. S1A). The data were plotted on a distribution graph, to compare global acetylation between the 2 conditions (Fig. 6A). Overall, these data show no obvious decrease of NTA level in the Tg*AT1-KO*. Next, we looked at the correlation of the NTA observed in the Tg*AT1-KO* with respect to those of the same proteoforms in the wild-type, either considering the total proteins set, or making the distinction between proteins that underwent methionine excision ("+NME") and the proteins that were NTAed on the Met or on downstream amino acids (Table S1). Again, we observed unmodified NTA yields in both conditions, regardless of the position of the modification or the nature of the modified residue. We concluded that deletion of Tg*AT1* had no impact on the N-terminal acetylomes in neither the cytosolic nor the ER compartment.

We also analyzed the *P. berghei* data under enriched gametocytes conditions, (72% gametocyte purity, 28% late trophozoites/schizonts) in the same AT1 deletion context and compared the data to the wildtype sample. As in the case of *T. gondii* samples, no alteration of N-terminal acetylome was observed in 2.34Pb*AT1-KO* compared to 2.34 wildtype gametocytes (Fig. 6A). In addition, as could be anticipated from the data already with the WT, the data of the mutant did not provide any additional information on the impact of NTA on secreted proteins. This could be due to (i) the very low number of proteins detected (4) with remote N-terminus caused by proteolytic cleavage and (ii) the absence of associated NTA in any of those proteins. All four entries (PBANKA_0201600, PBANKA_0619200, PBANKA_0501100, PBANKA_1334300), corresponding to ETRAMP, PSOP1, SEP2 and EXP2 proteins, display a signal peptide which was predicted to be cleaved. Among them, we observed that a secreted ookinete protein (PBANKA_0619200) displays a signal peptide featuring two cleavage sites in close proximity (positions 17 and 21), plausibly mediating entry into the secretory pathway. None of the neo-N-termini is N-acetylated. Nevertheless, newly formed N-termini of secreted proteins featuring NTA have been reported to occur in the ER of *P. falciparum* (Chang et al., 2008, Osborne et al., 2010).

Loss of TgAT1 modestly alters lysine acetylation of only a few proteins

To complete our results on the potential impact of blocking putative cytosolic acetyl-CoA import on acetylation of proteins, we probed the K-acetylome of *T. gondii* parasites lacking AT1 and compared it with the WT parasites using mass spectrometry (MS)-based label-free quantitative proteomic analyses. On the 313 K-acetylation sites reproducibly quantified and belonging to 200 different proteins (Table S5, Fig. 6B), three present on the same peptide of ribosomal protein RPS6 were found to be significantly hyperacetylated in the knock-out strain compared to the WT, along with one site in phosphofructokinase PFKII and one in dehydrogenase E1 component family protein (>2 fold and p-value<0.01) (Table S5, Fig. 6C). On the other hand, six lysines carried by six different proteins (GRA2, trypsin domain containing protein, AP2 domain transcription factor AP2X-7, and three hypothetical proteins) were found to be hypo-acylated in the knock-out strain compared to the WT (Table S5, Fig. 6C). We examined the subcellular localization of the differentially K-acetylated proteins as assigned by hyperLOPIT data (Barylyuk et al., 2020) and the

CRISPR/Cas9 based tachyzoite fitness prediction scores (Sidik et al., 2016). The hyper-acetylated ribosomal protein RPS6 is a 40S ribosome protein found in the cytosol and the AP2 domain transcription factor AP2X-7 have significant contribution to tachyzoite development based on a fitness score of -4.58 and -3.39 respectively (Fig. 6C, Table S5). The other three proteins localized to different secretory organelles and the Golgi and are predicted dispensable for tachyzoite development (Fig. 6C, Table S5). These findings suggest that TgAT1 is not a major driver of N-ε-lysine acetylation.

DISCUSSION

Acetylation is a major modification of proteins. K-acetylation is known as a prominent post-translational modification in malaria parasites (Doerig et al., 2015), plausibly due to the high content occurrence of lysine residues as a result of its AT rich genome (Chanda et al., 2005, Gardner et al., 2002). N-terminal α-acetylation (NTA) of proteins not only occurs co-translationally in the cytosol but also post-translationally at the Golgi and plastid (Giglione et al., 2015, Aksnes et al., 2019, Linster and Wirtz, 2018). NTA modification seems to be less frequent on ER translocated proteins and may be a modification inhibiting targeting of cytosolic proteins into the ER (Forte et al., 2011). In this report, we assigned most apicomplexan acetyltransferase catalytic subunits to their proper protein substrate specificity either in the cytosol (NatA/B/C/E), the nucleus (NatD) or the inner cytosol membrane network (NatF). The parasites have an unusually high level of protein acetylation in the ER, and this process occurs at various stages along ER protein maturation (Fig. 3A and Fig. S1B). The role of the acetyltransferase(s) involved in both KA and NTA activities as well as the acetyl-CoA supply within the ER were addressed.

The data suggest that the most likely candidate for ER protein acetylation is the NAT8 homolog, the only ER-resident Nat in *T. gondii*. TgNAT8 N-terminus could be mapped in the course of our analysis and shown to display an N-terminal acetylation on Ala2. This is a typical NatA (i.e., cytosolic) acetylation mark and absence of signal peptide cleavage further suggests that the N-terminus is most likely oriented towards the cytosol side as in mammals. With almost 300 residues, the disordered N-terminal cytosolic domain is however unusually large compared to the mammalian ones

(Farrugia and Puglielli, 2018, Ko and Puglielli, 2009) and its exact function is unknown. Like animal NAT8s, TgNAT8 displays a single transmembrane domain followed by the C-terminal GNAT acetyltransferase domain that is located within the ER lumen as a result. This domain relies on an acetyl-CoA fuel to promote protein acetylation in the ER. So far NAT8 is described to display Lysine acetylase activity in mammals; nevertheless, as many studies now acknowledge, increasing number of GNATs exhibiting both activities do exist (Bienvenut 2020, Giglione & Meinnel 2021, Meinnel et al. 2020). Therefore, one cannot exclude that TgNAT8 also displays N-terminal acetyltransferase activity. If TgNat8 does not display this activity, similarly to the NatH homolog which we could not identify in Toxoplasma, there are only four yet unassigned GNAT homologs to propose as candidates (Table S4). Alternatively, one could envisage that free NAA10 or NAA20 subunits variants for instance devoid of the ancillary subunits might be translocated in the ER.

In mammals, AT1 activity is essential for cell viability and regulates cytosolic acetyl-CoA levels and Nε-lysine acetylation of proteins in the secretory pathway, cytosol, nucleus and mitochondria (Dieterich et al., 2019, Jonas et al., 2010, Farrugia and Puglielli, 2018). Moreover, AT1 controls cell metabolism including lipids and mitochondria bioenergetics (Dieterich et al., 2019). AT1 was the most relevant candidate to supply acetyl-CoA in the ER. However, we did not observe a correlation between AT1 inactivation and K- or N-terminal acetylomes variations of ER-translocated proteins in Apicomplexa. This suggests the occurrence of an alternative source of acetyl-CoA supplying the ER in addition to AT1. This alternative source would be sufficient for the acetyltransferase catalyst(s) involved (e.g., NAT8) in the absence of AT1. In this context, alternative routes of acetyl-CoA import in the ER might occur for instance through the nuclear pore and the nucleus or through mitochondrion-ER (Mallo et al., 2021) or plastid-ER contact sites or through acetyl-carnitine or acetyl-aspartate exchange. AT1 could therefore be involved in the ER acetyl-CoA pool to increase its content beyond the minimal concentration which alternative processes could fulfill. In support of this hypothesis, depletion of cytosolic acetyl-CoA in yeast has been shown to have no impact on global NTA of cytosolic proteins (Varland et al., 2018, Cova et al., 2018). This suggests ER acetyltransferase(s) to be effective with low acetyl-CoA values (i.e. <5-25 µM, the average concentration in the cytosol (Pietrocola et al., 2015) and Km values of NATs in the same range (Farrugia and Puglielli, 2018). As it is still required for efficient

growth in apicomplexans without apparent effect on protein targets, our current data also suggest a supplementary import activity of AT1 in addition to acetyl-CoA import for protein acetylation. Whether this is related to other, higher range (i.e. >C2) acyl-CoA import or to other small compounds is yet unknown. Finally, as we identify few ER-resident targets but rather many post-Golgi targets, one cannot exclude that a transporter functionally similar to AT1 fuels with acetyl-CoA the secretory compartments downstream the Golgi. The very polarized secretory pathway of apicomplexan parasites required for cell invasion indeed mostly involves a directed gradient downstream the endolysosomal compartment (Sheiner and Soldati-Favre, 2008).

P. falciparum exported and secreted proteins are also processed and acetylated in the ER (Chang et al., 2008, Osborne et al., 2010), this work). In *Plasmodium*, increase of acetate/acetyl-CoA in the cytosol specifically up-regulates K-acetylation status of acetyltransferases, transcriptional, ribosomal and translation related proteins but it does not cause a generalized effect on the whole cellular K-acetylome (Cobbold et al., 2016). This indicates that the ER acetyl-CoA pool is not limiting for protein acetylation in this compartment. The molecular mechanisms governing specific metabolic requirement between female and male gametocytes in *Plasmodium* are elusive. Our results suggest a differential requirement for AT1 between females and males. Of interest are the nucleo-cytosol localized RNA/DNA binding ALBA proteins in *Plasmodium* spp. (Reddy et al., 2015, Vembar et al., 2015), whose functions are regulated by acetylation (Goyal et al., 2012). In *P. yoelii* absence of a member of the ALBA family, (ALBA4) has been shown to be deleterious to asexual forms development and activation of male gametocytes (Munoz et al., 2017). Proteome-wide K-acetylation analyses of this mutant may reveal substrates regulated by AT1 activity.

The different subcellular localization of the three investigated putative NATs in *T. gondii* align with the occurrence of NAT modifications in different compartments in eukaryotic cells ie cytosol, ER and nucleus. Nevertheless, unlike plants (Giglione & Meinnel 2021), while possessing a plastid, no plastid NAT could be identified in *T. gondii.* Deeper investigation of the NATs and N-termini characterization in the absence of the identified acetyltransferases (Table S4) would be required to fully appreciate the functionality of this modification in Apicomplexa.

MATERIALS AND METHODS

T. gondii parasite culture

T. gondii tachyzoites were grown in human foreskin fibroblasts (HFFs) purchased from American Type Culture Collection-ATCC (CRL-2088 Ref# CCD1072Sk). Dulbecco's Modified Eagle's Medium (DMEM, Gibco) supplemented with 5% fetal calf serum (FCS), 2 mM glutamine and 25 µg/ml gentamicin was used for maintenance of the cells. RHΔKu80 referred to as Tg or RH (Fox et al., 2009), RHΔKu80-Tir1 referred to as Tir (Brown et al., 2018) and RH-Dicre (Pieperhoff et al., 2015) strains were used as parental strains for generation of mutants.

Cloning of DNA and generation of constructs

Parasite genomic DNA (gDNA) was extracted using the Wizard SV genomic DNA purification kit (Promega). PCRs were done using the Q5 (New England Biolabs), GoTaq (Promega) and KOD (Novagen) polymerases with primers listed in supplementary table (Table S6) according to manufacturer's instructions. Cloning was done in E. coli XL-1 Gold chemo-competent bacteria.

Parasite transfection and selection of stable mutants

To generate CRISPR/Cas9 directed Tg*AT1-KO* strain, PCR was done using the Q5 site-directed mutagenesis kit on pSAG1::Cas9-U6::sgUPRT (Shen et al., 2014) vector as the template to produce double gRNA plasmid pSAG1::Cas9-U6::dgAT1 using primers 8723/8724 as previously described (Krishnan et al., 2020). DHFR cassette was amplified by KOD PCR using 5' and 3' primers 8725/8726 that hold 30 base pairs homology to *AT1* gene upstream and downstream of the two gRNAs.

To produce NAA30-mAID-Ty and NAT8-mAID-Ty strains, KOD PCR was done using primers 9994/9995 and 9984/9985 for the NAA30 and NAT8 respectively on vector pTub1-YFP:mAID:3Ty:DHFR:TS:HXGPRT as described in (Brown et al., 2018). NAT-UI-Dicre-Ty was generated using KOD PCR product produced using primers 9991/9992 with vector pG152:KI:3Ty:Lox:SAG1:3UTR:HXGPRT.GB as previously described (Pieperhoff et al., 2015). Single gRNAs for NAA30, NAT8 and NAT were produced by PCR using Q5 site directed mutagenesis on pSAG1::Cas9-U6::sgUPRT using primers 9993/4883, 9983/4883 and 9998/4883 for NAA30, NAT8 and NAT respectively to generate pSAG1::Cas9-U6::sgNAA30, pSAG1::Cas9-U6::sgNAT8 and pSAG1::Cas9-U6::sgNAT. The PCR products were precipitated in using sodium

acetate and ethanol and resuspended in 100µl of water prior to transfection. Co-transfections 30 µg of the gene specific gRNAs and respective KOD products in *T. gondii* tachyzoites were performed by electroporation as previously described (Soldati and Boothroyd, 1993). Resistant parasites were selected with appropriate drugs, either Mycophenolic acid (25 mg/mL) and xanthine (50 mg/mL) or pyrimethamine (1 µg/ml) for those carrying the HXGPRT (Donald et al., 1996) and DHFR cassettes (Donald and Roos, 1993) respectively. GoTaq PCR analyses were used to assess integration of DHFR cassette using primer pairs 8727/2017 for 5', 8728/2018 for 3' and deletion of *AT1* using 8727/8728. The NAA30-mAID-Ty, NAT8-mAID-Ty and NAT-UI-Dicre-Ty strains were confirmed by IFA and western blot assays upon induction of protein degradation with 1 mM auxin dissolved in ethanol or Rapamycin (Sigma) as appropriate. All primer sequences are listed in (Table S6).

Ethics statement

Experiments in mice were conducted under license number GE-30-13, according to the guidelines and regulations issued by the Swiss Federal Veterinary Office.

***P. berghei* maintenance, purification and transfection**

Maintenance and transfections in *P. berghei* were performed as previously described (Balestra et al., 2020). Briefly, *P. berghei* ANKA strain (Vincke and Lips, 1948), derived clones 2.34 (Billker et al., 2004), 820cl1 (Mair et al., 2010) and Pb*AT1-KO* parasites were grown and maintained in six-ten week old female CD1 outbred mice. The mice were housed in rooms kept at 21 ± 2 °C under a 12 h light/dark cycle. They were kept in individually ventilated cages and fed commercially prepared autoclaved dry rodent meals and water provided as often as necessary. Regular screenings were carried out on the mice to ensure a pathogen free status. Microscopy on methanol-fixed, thin blood smears stained with Giemsa was done to determine parasitemia of infected mice. Gametocyte production was enhanced by treatment of mice with phenylhydrazine three days prior to infection, followed by sulfadiazine (20 mg/L) treatment in drinking water a day post infection to clear the asexual forms. Exflagellation of male gametocytes was assessed on day 3 or four post infection by adding 4 µl of blood collected from a superficial tail vein to 70 µl exflagellation medium (RPMI 1640 containing 25 mM HEPES, 4 mM sodium bicarbonate, 5% fetal calf serum (FCS), 100 µM xanthurenic acid, pH 7.4. Exflagellation centres were

enumerated per 100 microgametocytes, the percentage of RBCs infected with microgametocytes was assessed on Giemsa-stained smears. Gametocyte purification was done by adding collected parasites to suspended animation medium - SA (SA; RPMI 1640 containing 25 mM HEPES, 5% FCS, 4 mM sodium bicarbonate, pH 7.20). This was followed by gradient separation from uninfected erythrocytes on a Histodenz (Sigma) solution made from 48% of a Histodenz stock (27.6% [w/v] Histodenz in 5.0 mM TrisHCl, 3.0 mM KCl, 0.3 mM EDTA, pH 7.20) and 52% SA, final pH 7.2 and collection of gametocytes from the interface.

To delete Pb*AT1, Not1* digestion was used to release the DNA insert from the backbone of PlasmoGem *AT1* knock out vector number PbGEM-265292 followed by ethanol precipitation of DNA. For transfections, parasites were collected from mice and grown overnight *in vitro*, the schizonts were then purified by gradient method, using Histodenz solution made from 55% of the Histodenz stock and 45% PBS. Schizonts were collected from the intermediate layer, centrifuged at 500 *g* for 3 min, resuspended in 25 µl Amaxa Basic Parasite Nucleofector solution (Lonza) containing 10-20 µg of DNA (knock out linear vector) dissolved in 10 µl H_2O.

Cells were electroporated using the FI-115 program of the Amaxa Nucleofector 4D. Transfected parasites were subsequently resuspended in 200 µl fresh erythrocytes and injected intraperitoneally into mice. Parasite selection was started one day post infection using 0.07 mg/mL pyrimethamine (Sigma) in the drinking water (pH ~4.5).

Genotyping was done using primers GW2/QCR2 and GW2/GT to check for integration of the vector into the locus, and QCR1/QCR2 and 6516/6517 primers to check for wildtype locus. Primers sequences used are listed in (Table S6).

Antibodies

The following antibodies were used in this study; rabbit polyclonal α-GAP45, mouse monoclonal α-Ty (BB2) as described before (Frenal et al., 2014, Plattner et al., 2008) Anti mouse α-tubulin clone DM1A product number T6199 purchased from Sigma-Aldrich. TER-119 monoclonal antibody was purchased from ThermoFisher cat # 12-5921-82. For immunofluorescence assays, Alexa Fluor 488, Alexa Fluor 594 and Alexa Fluor 680 conjugated to goat α-mouse or α-rabbit (Life Technologies) were used. For western blot analyses, secondary peroxidase conjugated goat α-rabbit or mouse antibodies (Sigma) were used.

Indirect immunofluorescence assay

Confluent HFF cells seeded on cover slips in 24-well plates were inoculated with test strains for 24 hours. This was followed by fixation with 4% PFA/0.05% glutaraldehyde (PFA/GA) in PBS and neutralization in 0.1M glycine/PBS for 3–5 min and processed with appropriate antibodies as previously described in (Plattner et al., 2008, Nyonda et al., 2020). Immunofluorescence of gametocytes were performed as previously described (Aurélia C. Balestra, 2020, Volkmann et al., 2012), briefly, purified gametocytes were fixed with 4% paraformaldehyde and 0.05% glutaraldehyde in PBS for 1 h. This was followed by permeabilization with 0.1% Triton X-100/PBS for 10 min and blocking step in 2% BSA/PBS for 2 h. Primary antibodies staining with α-tubulin and TER-119 (erythrocyte membrane marker) diluted 1:1000 in blocking buffer was done followed by secondary antibody staining. Confocal images were acquired with LSM800 Airyscan objective apochromat 63x/1.4 oil found at the Bioimaging core facility of the Faculty of Medicine, University of Geneva. Z-stack sections were processed using the ImageJ software.

Flow cytometry analysis on gametocytes

The DNA content of male gametocytes was measured as previously described (Fang et al., 2017). Purified gametocytes were resuspended in 100µl of SA medium and activation induced by adding 100 µl of modified exflagellation medium (RPMI 1640 containing 25 mM HEPES, 4 mM sodium bicarbonate, 5% FCS, 200 µM xanthurenic acid, pH 7.8). 800 µl of ice-cold PBS was rapidly added to the cells to inhibit gametogenesis and cells stained for 30 min at 4°C with Vybrant dye cycle (Life Technologies) then analyzed on Beckman Coulter Gallios 4. Male gametocytes were selected on fluorescence by gating on GFP positive cells while female gametocytes on RFP positive cells in the 820cl1 wildtype and derived Pb*AT1-KO* parasites. Percentage of micro and macro gametocytes was expressed as a percentage of all parasite stages including asexual forms while DNA replication status was expressed as a percentage of male gametocytes only. For each sample, >20,000 cells were analysed.

Western blot analysis

Freshly egressed parasites were pelleted and resuspended in RIPA buffer (150 mM NaCl, 1% Triton X-100, 0.5% deoxycholate, 0.1% SDS, 50 mM Tris pH 7.5 plus protease inhibitor) and incubated on ice for 15 minutes. This was followed by centrifugation at 14,000 r.p.m. at 4 °C for 15 minutes. The supernatant was separated from the pellet in a fresh tube and mixed with SDS–PAGE loading buffer under reducing conditions. The preparations were transferred on to nitrocellulose membranes and probed with appropriate antibodies in 5% non-fat milk powder dissolved in PBS-0.05% Tween20. Proteins were detected through bound secondary peroxidase-conjugated antibodies using the ECL systems (Amersham).

Intracellular growth

Confluent HFFs on coverslips were inoculated with the test strains and controls and let to grow for 24 hours. The infected cells were fixed using PFA/GA and IFAs followed using α-GAP45 antibodies. The experiment was repeated three independent times and one hundred vacuoles enumerated in each experiment. The data are presented as mean ± *SD*.

Lysis plaque assay

HFFs were seeded into confluency and subsequently inoculated with freshly egressed parasites. The infected cells were allowed to sit for 7 days and then fixed using PFA/GA and plaque sizes revealed by 0.1% crystal violet (Sigma) staining.

Parasite growth competition assay

In *P. berghei***,** Pb*AT1-KO* parasites derived from the 820cl1 line and wildtype parasite of 2.34 line were mixed in a 5:1 ratio respectively and infected intraperitoneally into mice. Parasitemia was determined daily by flowcytometry and gating was done for Pb*AT1-KO* parasites based on fluorescence expression. Mice were sacrificed 6 days post infection based on total parasitemia.

In *T. gondii,* Tg*AT1-KO* and RH (Tg) were each mixed with GFP expressing parasites at an estimated ratio of 80:20 (test strain: GFP strain). HFFs were inoculated with this mixture and parasite ratios determined by flow cytometry at each passage as previously described (Nyonda et al., 2020)

MS-based quantitative proteomic analysis of K-acetylome

Sample preparation

Five replicates of wild-type and *AT1*-KO freshly egressed parasites were lysed from host cells by repeatedly by passage through syringe (3x 28G) and subsequently purified through filtration (3µm pore size, Millipore/Merck). The parasites were subsequently pelleted at 2800 g, for 20 minutes at 4ºC. 1ml of ice cold 8M urea in 50mM HEPES buffer with protease inhibitor at pH 6.6 was then added to the pellets and resuspended gently using a pipette. This was followed by a sonication step of the samples at 4°C in an ultrasonic bath for 10 cycles (10 seconds sonication on and 30 seconds sonication off) and immediately transferred on ice. Extracted proteins were reduced using 20mM of dithiothreitol for 1 h at 37 °C before alkylation with 55mM of iodoacetamide for 45 min at room temperature in the dark. The samples were then diluted using ammonium bicarbonate to obtain a urea concentration of 4M. Proteins were digested with LysC (Promega) at a ratio of 1:200 during 4 h at 37 °C. The samples were diluted again using ammonium bicarbonate to obtain a urea concentration of 1 M. Proteins were then digested with Trypsin (Promega) at a ratio of 1:200 overnight at 37 °C. Resulting peptides were purified by C18 reverse phase chromatography (Sep-Pak C18, Waters) before drying down.

Enrichment of acetylated peptides

Dried peptides were dissolved in IP buffer (100 mM NaCl, 1mM EDTA, 20 mM Tris-HCl, 0.5 % NP-40, pH 8). Acetylated peptides were mixed with anti–acetyl-lysine antibody immobilized on agarose beads (ImmuneChem-ICP0388) and incubated overnight at 4 °C. Following incubation, the beads were washed twice with IP buffer, once with washing buffer (IP buffer without NP-40) and twice with ice cold ultra-pure water. Elution was performed using 0.1 % TFA. Enriched peptides were then dried down.

NanoLC-MS/MS analyses

The peptides were analyzed by online nanoliquid chromatography coupled to MS/MS (Ultimate 3000 RSLCnano coupled to a Q-Exactive HF, Thermo Fisher Scientific) using a 120-min gradient. Peptides were sampled on a 300 µm × 5 mm PepMap C18 precolumn and separated on a 75 µm x 250 mm C18 column (Reprosil-Pur 120 C18-

AQ, 1.9 µm, Dr. Maisch). MS and MS/MS data were acquired using the Xcalibur software (Thermo Scientific).

Acetylated sites identification and quantification

RAW files were processed using MaxQuant (Tyanova et al., 2016). Spectra were searched against the *T. gondii* database (ME49 taxonomy, version 30 downloaded from ToxoDB, the Uniprot database (*Homo sapiens* taxonomy, 2020-11-27 version), the frequently observed contaminants database embedded in MaxQuant, and the corresponding reverse databases. Trypsin was chosen as the enzyme and six missed cleavages were allowed. Precursor and fragment mass error tolerances were set at their default values. Peptide modifications allowed during the search were: Carbamidomethyl (C, fixed), Acetyl (Protein N-term, variable), Oxidation (M, variable) and Acetyl (K, variable). Minimum number of peptides and razor + unique peptides were set to 1. Maximum false discovery rates were set to 0.01 at PSM, protein and site levels. The match between runs option was activated.

Statistical analyses

Statistical analyses were performed using ProStaR (Wieczorek et al., 2017). Only acetylated sites with a localization probability above 0.75 were considered. Peptides identified in the reverse and contaminant databases were discarded. For the comparison of acetylomes between the mutant strain and WT strains, acetylated sites were split into several lanes when they were identified on peptides bearing various numbers of acetylated sites to allow the quantification of the different peptidoforms. Only acetylated sites quantified in at least 4 replicates of one condition were conserved. After log2 transformation, acetylated site intensities were normalized using the vsn method before missing value imputation (slsa algorithm for partially observed values in the condition and DetQuantile algorithm for totally absent values in the condition). Statistical testing was conducted using limma. Differentially abundant acetylated sites were sorted out using the following cut-offs: log2(fold change) ≥ 1 or ≤ -1 and p-value < 0.01, leading to a false discovery rate < 1% according to the Benjamini-Hochberg estimator. Acetylated sites found differentially abundant but identified by MS/MS in less than three replicates and detected in less than four replicates in the condition in which they were found to be more abundant were invalidated (p-value = 1).

N-terminomics

The parasite pellets were resuspended in 0.2 mL of lysis buffer consisting of 50 mM HEPES/NaOH pH 7.2; 1.5 mM MgCl2; 1 mM EGTA; 10% glycerol; 1% triton X-100; 2 mM PMSF; EDTA+ protease inhibitor. The protein were briefly sonicated to ensure proper lysis, then incubated at 4°C for 1 hour. Samples were centrifuged 60 min at 4°C and 17 000 g, the supernatants were collected and the protein amounts quantified using the Bradford method. 500 µg were then processed as described (Bienvenut et al., 2017) with the exception of a few modifications detailed bellow. Briefly, the proteins extracted from the biological material were labelled on their N-termini and lysine ε-amino groups using N-acetoxy-[2H3] succinimide, before being subjected to trypsin digestion. The peptides obtained were then fractionated on a Strong Cation eXchange chromatography, and the fractions number 2-11 were individually analysed on an LTQ-Orbitrap velos mass spectrometer (Thermo) coupled to a liquid chromatography. The data obtained were processed using Mascot Distiller, respectively searching against a custom “ME49”-based *T. gondii* protein database (v.30) or a *P. berghei* reference proteome set (UP000074855), with the parent and fragment mass tolerance respectively defined to 10 ppm and 0.5 Da. The quantitation results, along with each Mascot search output, were then parsed using the EnCOUNTer script to obtain the final N-ter acetylome datasets. The analyzed samples corresponded to the RHΔKU80 *T. gondii* strain (“WT”), and the *AT1*-KO mutant (Tg*AT1*-KO), and to the ANKA *P. berghei* strain as well as the corresponding *AT1*-KO mutant (Pb*AT1*-KO), with respectively either three or two distinct biological replicates of each condition.

Acknowledgements

The authors thank Jean-Baptiste Marq and Aurelia Balestra for technical assistance. We thank the Bioimaging and Flow Cytometry core facilities at the Faculty of Medicine Geneva.

Competing interests

The authors declare no competing interests

Author contributions

Conceptualization, D.S-F., C.G. and T.M; Methodology design**,** M.A.N., P.P., M.B., L.B., JB.B., Y.C., D.S-F., C.G. and T.M.; Formal analysis, M.A.N., P.P., M.B, L.B., Y.C., JB.B., D.S-F., C.G. and T.M; Investigation, M.A.N., P.P., A.K., M.B, L.B., Y.C., JB.B., C.G. and T.M.; Writing original draft, M.A.N., C.G. and T.M.; Writing-Review and Editing, M.A.N., P.P., A.K., M.B, L.B., Y.C., C.G. and T.M; Visualization, M.A.N., A.K., C.G. and T.M; Supervision, D.S-F., C.G. and T.M ; Project administration, M.A.N., C.G. and T.M ; Funding acquisition, D.S-F, C.G. and T.M.

Funding

This research was supported by European Research Council (ERC) under the European Union's Horizon 2020 research and innovation program agreement no.695596 to D.S-F., by 51RTP0_151032 (MalarX), a SystemsX grant awarded by the Swiss National Science foundation to D.S-F., by KatNat (ERA-NET, ANR-17-CAPS-0001-01) and CanMore (France-Germany PRCI, ANR-20 CE92-0040) grants funded by French National Research Agency (ANR) to CG to support JB.B, by Foundation ARC (ARCPJA32020060002137) grants to TM, and from the facilities and expertise of the I2BC proteomic platform SICaPS, supported by IBiSA, Ile de France Region, Plan Cancer, CNRS and Paris-Sud University. The proteomic experiments were partially supported by Agence Nationale de la Recherche under projects ProFI (Proteomics French Infrastructure, ANR-10-INBS-08) and GRAL, a program from the Chemistry Biology Health (CBH) Graduate School of University Grenoble Alpes (ANR-17-EURE-0003).

Data availability

Toxoplasma gondii transgenic strains are available upon request.

The published article includes all datasets generated or analyzed during this study. Mass spectrometry proteomics data associated to the N-terminal and lysine

acetylomes have been deposited to the ProteomeXchange Consortium (http://proteomecentral.protemeexchange.org) via the PRIDE repository (https://www.ebi.ac.uk/pride/; (Vizcaíno et al., 2013)) with the dataset identifiers: PXD029616 (Username: reviewer_rpxd029616@ebi.ac.uk, Password: ReQZ5fU5) and PXD030932 (Username: reviewer_pxd030932@ebi.ac.uk, Password: B0yNgS97). The corresponding datasets (Tables S1, S2 and S5) are available at the figshare repository (https://figshare.com/) with DOIs 10.6084/m9.figshare.19723183, 10.6084/m9.figshare.19723201 and 10.6084/m9.figshare.19723237.

REFERENCES

Aksnes, H., Drazic, A., Marie, M. & Arnesen, T. 2016. First Things First: Vital Protein Marks by N-Terminal Acetyltransferases. *Trends Biochem Sci,* 41**,** 746-760.

Aksnes, H., Ree, R. & Arnesen, T. 2019. Co-translational, Post-translational, and Non-catalytic Roles of N-Terminal Acetyltransferases. *Mol Cell,* 73**,** 1097-1114.

Aurélia C. Balestra, K. K., Natacha Klages, Steven A. Howell, Helen R. Flynn, Marcus Bantscheff, Carla Pasquarello, Abigail J. Perrin, Lorenzo Brusini, Patrizia Arboit, Olalla Sanz, Laura Peces-Barba Castaño, Chrislaine Withers-Martinez, Alexandre Hainard, Sonja Ghidelli-Disse, Ambrosius P. Snijders, David A. Baker, Michael J. Blackman, Mathieu Brochet 2020. A multipass membrane protein interacts with the cGMP-dependent protein kinase to regulate critical calcium signals in malaria parasites. *bioRxiv,* 2020.07.18.209973.

Balestra, A. C., Zeeshan, M., Rea, E., Pasquarello, C., Brusini, L., Mourier, T., Subudhi, A. K., Klages, N., Arboit, P., Pandey, R., Brady, D., Vaughan, S., Holder, A. A., Pain, A., Ferguson, D. J., Hainard, A., Tewari, R. & Brochet, M. 2020. A divergent cyclin/cyclin-dependent kinase complex controls the atypical replication of a malaria parasite during gametogony and transmission. *Elife,* 9.

Barylyuk, K., Koreny, L., Ke, H., Butterworth, S., Crook, O. M., Lassadi, I., Gupta, V., Tromer, E., Mourier, T., Stevens, T. J., Breckels, L. M., Pain, A., Lilley, K. S. & Waller, R. F. 2020. A Comprehensive Subcellular Atlas of the *Toxoplasma*

Proteome via hyperLOPIT Provides Spatial Context for Protein Functions. *Cell Host Microbe,* 28**,** 752-766 e9.

Bienvenut, W. V., Brunje, A., Boyer, J. B., Muhlenbeck, J. S., Bernal, G., Lassowskat, I., Dian, C., Linster, E., Dinh, T. V., Koskela, M. M., Jung, V., Seidel, J., Schyrba, L. K., Ivanauskaite, A., Eirich, J., Hell, R., Schwarzer, D., Mulo, P., Wirtz, M., Meinnel, T., Giglione, C. & Finkemeier, I. 2020. Dual lysine and N-terminal acetyltransferases reveal the complexity underpinning protein acetylation. *Mol Syst Biol,* 16**,** e9464.

Bienvenut, W. V., Giglione, C. & Meinnel, T. 2015. Proteome-wide analysis of the amino terminal status of Escherichia coli proteins at the steady-state and upon deformylation inhibition. *Proteomics,* 15**,** 2503-18.

Bienvenut, W. V., Giglione, C. & Meinnel, T. 2017. SILProNAQ: A Convenient Approach for Proteome-Wide Analysis of Protein N-Termini and N-Terminal Acetylation Quantitation. *Methods Mol Biol,* 1574**,** 17-34.

Billker, O., Dechamps, S., Tewari, R., Wenig, G., Franke-Fayard, B. & Brinkmann, V. 2004. Calcium and a calcium-dependent protein kinase regulate gamete formation and mosquito transmission in a malaria parasite. *Cell,* 117**,** 503-14.

Billker, O., Lindo, V., Panico, M., Etienne, A. E., Paxton, T., Dell, A., Rogers, M., Sinden, R. E. & Morris, H. R. 1998. Identification of xanthurenic acid as the putative inducer of malaria development in the mosquito. *Nature,* 392**,** 289-92.

Boddey, J. A., Hodder, A. N., Gunther, S., Gilson, P. R., Patsiouras, H., Kapp, E. A., Pearce, J. A., De Koning-Ward, T. F., Simpson, R. J., Crabb, B. S. & Cowman, A. F. 2010. An aspartyl protease directs malaria effector proteins to the host cell. *Nature,* 463**,** 627-31.

Brown, K. M., Long, S. & Sibley, L. D. 2018. Conditional Knockdown of Proteins Using Auxin-inducible Degron (AID) Fusions in *Toxoplasma gondii*. *Bio Protoc,* 8.

Bushell, E., Gomes, A. R., Sanderson, T., Anar, B., Girling, G., Herd, C., Metcalf, T., Modrzynska, K., Schwach, F., Martin, R. E., Mather, M. W., Mcfadden, G. I., Parts, L., Rutledge, G. G., Vaidya, A. B., Wengelnik, K., Rayner, J. C. & Billker, O. 2017. Functional Profiling of a *Plasmodium* Genome Reveals an Abundance of Essential Genes. *Cell,* 170**,** 260-272 e8.

Caldelari, R., Dogga, S., Schmid, M. W., Franke-Fayard, B., Janse, C. J., Soldati-Favre, D. & Heussler, V. 2019. Transcriptome analysis of *Plasmodium berghei* during exo-erythrocytic development. *Malar J,* 18**,** 330.

Chanda, I., Pan, A. & Dutta, C. 2005. Proteome composition in *Plasmodium falciparum*: higher usage of GC-rich nonsynonymous codons in highly expressed genes. *J Mol Evol,* 61**,** 513-23.

Chang, H. H., Falick, A. M., Carlton, P. M., Sedat, J. W., Derisi, J. L. & Marletta, M. A. 2008. N-terminal processing of proteins exported by malaria parasites. *Mol Biochem Parasitol,* 160**,** 107-15.

Cobbold, S. A., Santos, J. M., Ochoa, A., Perlman, D. H. & Llinas, M. 2016. Proteome-wide analysis reveals widespread lysine acetylation of major protein complexes in the malaria parasite. *Sci Rep,* 6**,** 19722.

Cobbold, S. A., Vaughan, A. M., Lewis, I. A., Painter, H. J., Camargo, N., Perlman, D. H., Fishbaugher, M., Healer, J., Cowman, A. F., Kappe, S. H. & Llinas, M. 2013. Kinetic flux profiling elucidates two independent acetyl-CoA biosynthetic pathways in *Plasmodium falciparum*. *J Biol Chem,* 288**,** 36338-50.

Coffey, M. J., Dagley, L. F., Seizova, S., Kapp, E. A., Infusini, G., Roos, D. S., Boddey, J. A., Webb, A. I. & Tonkin, C. J. 2018. Aspartyl Protease 5 Matures Dense Granule Proteins That Reside at the Host-Parasite Interface in *Toxoplasma gondii*. *mBio,* 9.

Coffey, M. J., Sleebs, B. E., Uboldi, A. D., Garnham, A., Franco, M., Marino, N. D., Panas, M. W., Ferguson, D. J., Enciso, M., O'neill, M. T., Lopaticki, S., Stewart, R. J., Dewson, G., Smyth, G. K., Smith, B. J., Masters, S. L., Boothroyd, J. C., Boddey, J. A. & Tonkin, C. J. 2015. An aspartyl protease defines a novel pathway for export of *Toxoplasma* proteins into the host cell. *Elife,* 4.

Cova, M., Lopez-Gutierrez, B., Artigas-Jeronimo, S., Gonzalez-Diaz, A., Bandini, G., Maere, S., Carretero-Paulet, L. & Izquierdo, L. 2018. The Apicomplexa-specific glucosamine-6-phosphate N-acetyltransferase gene family encodes a key enzyme for glycoconjugate synthesis with potential as therapeutic target. *Sci Rep,* 8**,** 4005.

De Vries, L. E., Lunghi, M., Krishnan, A., Kooij, T. W. A. & Soldati-Favre, D. 2021. Pantothenate and CoA biosynthesis in Apicomplexa and their promise as antiparasitic drug targets. *PLoS Pathog,* 17**,** e1010124.

Dieterich, I. A., Lawton, A. J., Peng, Y., Yu, Q., Rhoads, T. W., Overmyer, K. A., Cui, Y., Armstrong, E. A., Howell, P. R., Burhans, M. S., Li, L., Denu, J. M., Coon, J. J., Anderson, R. M. & Puglielli, L. 2019. Acetyl-CoA flux regulates the proteome and acetyl-proteome to maintain intracellular metabolic crosstalk. *Nat Commun,* 10**,** 3929.

Doerig, C., Rayner, J. C., Scherf, A. & Tobin, A. B. 2015. Post-translational protein modifications in malaria parasites. *Nat Rev Microbiol,* 13**,** 160-72.

Dogga, S. K., Mukherjee, B., Jacot, D., Kockmann, T., Molino, L., Hammoudi, P. M., Hartkoorn, R. C., Hehl, A. B. & Soldati-Favre, D. 2017. A druggable secretory protein maturase of *Toxoplasma* essential for invasion and egress. *Elife,* 6.

Donald, R. G., Carter, D., Ullman, B. & Roos, D. S. 1996. Insertional tagging, cloning, and expression of the *Toxoplasma gondii* hypoxanthine-xanthine-guanine phosphoribosyltransferase gene. Use as a selectable marker for stable transformation. *J Biol Chem,* 271**,** 14010-9.

Donald, R. G. & Roos, D. S. 1993. Stable molecular transformation of *Toxoplasma gondii:* a selectable dihydrofolate reductase-thymidylate synthase marker based on drug-resistance mutations in malaria. *Proc Natl Acad Sci U S A,* 90**,** 11703-7.

Fang, H., Klages, N., Baechler, B., Hillner, E., Yu, L., Pardo, M., Choudhary, J. & Brochet, M. 2017. Multiple short windows of calcium-dependent protein kinase 4 activity coordinate distinct cell cycle events during *Plasmodium* gametogenesis. *Elife,* 6.

Farrugia, M. A. & Puglielli, L. 2018. Nepsilon-lysine acetylation in the endoplasmic reticulum - a novel cellular mechanism that regulates proteostasis and autophagy. *J Cell Sci,* 131.

Fleige, T., Fischer, K., Ferguson, D. J., Gross, U. & Bohne, W. 2007. Carbohydrate metabolism in the Toxoplasma gondii apicoplast: localization of three glycolytic isoenzymes, the single pyruvate dehydrogenase complex, and a plastid phosphate translocator. *Eukaryot Cell,* 6**,** 984-96.

Forte, G. M., Pool, M. R. & Stirling, C. J. 2011. N-terminal acetylation inhibits protein targeting to the endoplasmic reticulum. *PLoS Biol,* 9**,** e1001073.

Fox, B. A., Ristuccia, J. G., Gigley, J. P. & Bzik, D. J. 2009. Efficient gene replacements in *Toxoplasma gondii* strains deficient for nonhomologous end joining. *Eukaryot Cell,* 8**,** 520-9.

Frenal, K., Marq, J. B., Jacot, D., Polonais, V. & Soldati-Favre, D. 2014. Plasticity between MyoC- and MyoA-glideosomes: an example of functional compensation in *Toxoplasma gondii* invasion. *PLoS Pathog,* 10**,** e1004504.

Frottin, F., Bienvenut, W. V., Bignon, J., Jacquet, E., Vaca Jacome, A. S., Van Dorsselaer, A., Cianferani, S., Carapito, C., Meinnel, T. & Giglione, C. 2016. MetAP1 and MetAP2 drive cell selectivity for a potent anti-cancer agent in synergy, by controlling glutathione redox state. *Oncotarget,* 7**,** 63306-63323.

Frottin, F., Espagne, C., Traverso, J. A., Mauve, C., Valot, B., Lelarge-Trouverie, C., Zivy, M., Noctor, G., Meinnel, T. & Giglione, C. 2009. Cotranslational proteolysis dominates glutathione homeostasis to support proper growth and development. *Plant Cell,* 21**,** 3296-314.

Gardner, M. J., Hall, N., Fung, E., White, O., Berriman, M., Hyman, R. W., Carlton, J. M., Pain, A., Nelson, K. E., Bowman, S., Paulsen, I. T., James, K., Eisen, J. A., Rutherford, K., Salzberg, S. L., Craig, A., Kyes, S., Chan, M. S., Nene, V., Shallom, S. J., Suh, B., Peterson, J., Angiuoli, S., Pertea, M., Allen, J., Selengut, J., Haft, D., Mather, M. W., Vaidya, A. B., Martin, D. M., Fairlamb, A. H., Fraunholz, M. J., Roos, D. S., Ralph, S. A., Mcfadden, G. I., Cummings, L. M., Subramanian, G. M., Mungall, C., Venter, J. C., Carucci, D. J., Hoffman, S. L., Newbold, C., Davis, R. W., Fraser, C. M. & Barrell, B. 2002. Genome sequence of the human malaria parasite *Plasmodium falciparum*. *Nature,* 419**,** 498-511.

Giglione, C., Fieulaine, S. & Meinnel, T. 2015. N-terminal protein modifications: Bringing back into play the ribosome. *Biochimie,* 114**,** 134-46.

Giglione, C. & Meinnel, T. 2021. Evolution-Driven Versatility of N Terminal Acetylation in Photoautotrophs. *Trends Plant Sci*.

Goyal, M., Alam, A., Iqbal, M. S., Dey, S., Bindu, S., Pal, C., Banerjee, A., Chakrabarti, S. & Bandyopadhyay, U. 2012. Identification and molecular characterization of an Alba-family protein from human malaria parasite *Plasmodium falciparum*. *Nucleic Acids Res,* 40**,** 1174-90.

Hammoudi, P. M., Jacot, D., Mueller, C., Di Cristina, M., Dogga, S. K., Marq, J. B., Romano, J., Tosetti, N., Dubrot, J., Emre, Y., Lunghi, M., Coppens, I., Yamamoto, M., Sojka, D., Pino, P. & Soldati-Favre, D. 2015. Fundamental Roles of the Golgi-Associated *Toxoplasma* Aspartyl Protease, ASP5, at the Host-Parasite Interface. *PLoS Pathog,* 11**,** e1005211.

Hirabayashi, Y., Kanamori, A., Nomura, K. H. & Nomura, K. 2004. The acetyl-CoA transporter family SLC33. *Pflugers Arch,* 447**,** 760-2.

Hirabayashi, Y., Nomura, K. H. & Nomura, K. 2013. The acetyl-CoA transporter family SLC33. *Mol Aspects Med,* 34**,** 586-9.

Jeffers, V. & Sullivan, W. J., Jr. 2012. Lysine acetylation is widespread on proteins of diverse function and localization in the protozoan parasite *Toxoplasma gondii*. *Eukaryot Cell,* 11**,** 735-42.

Jonas, M. C., Pehar, M. & Puglielli, L. 2010. AT-1 is the ER membrane acetyl-CoA transporter and is essential for cell viability. *J Cell Sci,* 123**,** 3378-88.

Kloehn, J., Oppenheim, R. D., Siddiqui, G., De Bock, P. J., Kumar Dogga, S., Coute, Y., Hakimi, M. A., Creek, D. J. & Soldati-Favre, D. 2020. Multi-omics analysis delineates the distinct functions of sub-cellular acetyl-CoA pools in *Toxoplasma gondii*. *BMC Biol,* 18**,** 67.

Ko, M. H. & Puglielli, L. 2009. Two endoplasmic reticulum (ER)/ER Golgi intermediate compartment-based lysine acetyltransferases post-translationally regulate BACE1 levels. *J Biol Chem,* 284**,** 2482-92.

Krishnan, A., Kloehn, J., Lunghi, M., Chiappino-Pepe, A., Waldman, B. S., Nicolas, D., Varesio, E., Hehl, A., Lourido, S., Hatzimanikatis, V. & Soldati-Favre, D. 2020. Functional and Computational Genomics Reveal Unprecedented Flexibility in Stage-Specific *Toxoplasma* Metabolism. *Cell Host Microbe,* 27**,** 290-306 e11.

Lim, M. Y., Lamonte, G., Lee, M. C. S., Reimer, C., Tan, B. H., Corey, V., Tjahjadi, B. F., Chua, A., Nachon, M., Wintjens, R., Gedeck, P., Malleret, B., Renia, L., Bonamy, G. M. C., Ho, P. C., Yeung, B. K. S., Chow, E. D., Lim, L., Fidock, D. A., Diagana, T. T., Winzeler, E. A. & Bifani, P. 2016. UDP-galactose and acetyl-CoA transporters as *Plasmodium* multidrug resistance genes. *Nat Microbiol,* 1**,** 16166.

Linster, E. & Wirtz, M. 2018. N-terminal acetylation: an essential protein modification emerges as an important regulator of stress responses. *J Exp Bot,* 69**,** 4555-4568.

Mair, G. R., Lasonder, E., Garver, L. S., Franke-Fayard, B. M., Carret, C. K., Wiegant, J. C., Dirks, R. W., Dimopoulos, G., Janse, C. J. & Waters, A. P. 2010. Universal features of post-transcriptional gene regulation are critical for *Plasmodium* zygote development. *PLoS Pathog,* 6**,** e1000767.

Mak, A. B., Pehar, M., Nixon, A. M., Williams, R. A., Uetrecht, A. C., Puglielli, L. & Moffat, J. 2014. Post-translational regulation of CD133 by ATase1/ATase2-mediated lysine acetylation. *J Mol Biol,* 426**,** 2175-82.

Mallo, N., Ovciarikova, J., Martins-Duarte, E. S., Baehr, S. C., Biddau, M., Wilde, M. L., Uboldi, A. D., Lemgruber, L., Tonkin, C. J., Wideman, J. G., Harding, C. R. & Sheiner, L. 2021. Depletion of a *Toxoplasma* porin leads to defects in mitochondrial morphology and contacts with the endoplasmic reticulum. *J Cell Sci,* 134.

Martinez, A., Traverso, J. A., Valot, B., Ferro, M., Espagne, C., Ephritikhine, G., Zivy, M., Giglione, C. & Meinnel, T. 2008. Extent of N-terminal modifications in cytosolic proteins from eukaryotes. *Proteomics,* 8**,** 2809-31.

Munoz, E. E., Hart, K. J., Walker, M. P., Kennedy, M. F., Shipley, M. M. & Lindner, S. E. 2017. ALBA4 modulates its stage-specific interactions and specific mRNA fates during *Plasmodium yoelii* growth and transmission. *Mol Microbiol,* 106**,** 266-284.

Nyonda, M. A., Hammoudi, P. M., Ye, S., Maire, J., Marq, J. B., Yamamoto, M. & Soldati-Favre, D. 2020. *Toxoplasma gondii* GRA60 is an effector protein that modulates host cell autonomous immunity and contributes to virulence. *Cell Microbiol***,** e13278.

Osborne, A. R., Speicher, K. D., Tamez, P. A., Bhattacharjee, S., Speicher, D. W. & Haldar, K. 2010. The host targeting motif in exported *Plasmodium* proteins is cleaved in the parasite endoplasmic reticulum. *Mol Biochem Parasitol,* 171**,** 25-31.

Pehar, M. & Puglielli, L. 2013. Lysine acetylation in the lumen of the ER: a novel and essential function under the control of the UPR. *Biochim Biophys Acta,* 1833**,** 686-97.

Pieperhoff, M. S., Pall, G. S., Jimenez-Ruiz, E., Das, S., Melatti, C., Gow, M., Wong, E. H., Heng, J., Muller, S., Blackman, M. J. & Meissner, M. 2015. Conditional U1 Gene Silencing in *Toxoplasma gondii*. *PLoS One,* 10**,** e0130356.

Pietrocola, F., Galluzzi, L., Bravo-San Pedro, J. M., Madeo, F. & Kroemer, G. 2015. Acetyl coenzyme A: a central metabolite and second messenger. *Cell Metab,* 21**,** 805-21.

Plattner, F., Yarovinsky, F., Romero, S., Didry, D., Carlier, M. F., Sher, A. & Soldati-Favre, D. 2008. *Toxoplasma* profilin is essential for host cell invasion and TLR11-dependent induction of an interleukin-12 response. *Cell Host Microbe,* 3**,** 77-87.

Rathore, O. S., Faustino, A., Prudencio, P., Van Damme, P., Cox, C. J. & Martinho, R. G. 2016. Absence of N-terminal acetyltransferase diversification during evolution of eukaryotic organisms. *Sci Rep,* 6**,** 21304.

Reddy, B. P., Shrestha, S., Hart, K. J., Liang, X., Kemirembe, K., Cui, L. & Lindner, S. E. 2015. A bioinformatic survey of RNA-binding proteins in *Plasmodium*. *BMC Genomics,* 16**,** 890.

Russo, I., Babbitt, S., Muralidharan, V., Butler, T., Oksman, A. & Goldberg, D. E. 2010. Plasmepsin V licenses *Plasmodium* proteins for export into the host erythrocyte. *Nature,* 463**,** 632-6.

Sheiner, L. and Soldati-Favre, D. (2008). Protein trafficking inside Toxoplasma gondii. Traffic 9, 636-46.

Shen, B., Brown, K. M., Lee, T. D. & Sibley, L. D. 2014. Efficient gene disruption in diverse strains of *Toxoplasma gondii* using CRISPR/CAS9. *mBio,* 5**,** e01114-14.

Sidik, S. M., Huet, D., Ganesan, S. M., Huynh, M. H., Wang, T., Nasamu, A. S., Thiru, P., Saeij, J. P. J., Carruthers, V. B., Niles, J. C. & Lourido, S. 2016. A Genome-wide CRISPR Screen in *Toxoplasma* Identifies Essential Apicomplexan Genes. *Cell,* 166**,** 1423-1435 e12.

Soldati, D. & Boothroyd, J. C. 1993. Transient transfection and expression in the obligate intracellular parasite *Toxoplasma gondii*. *Science,* 260**,** 349-52.

Stanway, R. R., Bushell, E., Chiappino-Pepe, A., Roques, M., Sanderson, T., Franke-Fayard, B., Caldelari, R., Golomingi, M., Nyonda, M., Pandey, V., Schwach, F., Chevalley, S., Ramesar, J., Metcalf, T., Herd, C., Burda, P. C., Rayner, J. C., Soldati-Favre, D., Janse, C. J., Hatzimanikatis, V., Billker, O. & Heussler, V. T. 2019. Genome-Scale Identification of Essential Metabolic Processes for Targeting the *Plasmodium* Liver Stage. *Cell,* 179**,** 1112-1128 e26.

Talman, A. M., Domarle, O., Mckenzie, F. E., Ariey, F. & Robert, V. 2004. Gametocytogenesis: the puberty of *Plasmodium falciparum*. *Malar J,* 3**,** 24.

Tyanova, S., Temu, T. & Cox, J. 2016. The MaxQuant computational platform for mass spectrometry-based shotgun proteomics. *Nat Protoc,* 11**,** 2301-2319.

Tymoshenko, S., Oppenheim, R. D., Agren, R., Nielsen, J., Soldati-Favre, D. & Hatzimanikatis, V. 2015. Metabolic Needs and Capabilities of *Toxoplasma gondii* through Combined Computational and Experimental Analysis. *PLoS Comput Biol,* 11**,** e1004261.

Varland, S., Aksnes, H., Kryuchkov, F., Impens, F., Van Haver, D., Jonckheere, V., Ziegler, M., Gevaert, K., Van Damme, P. & Arnesen, T. 2018. N-terminal Acetylation Levels Are Maintained During Acetyl-CoA Deficiency in *Saccharomyces cerevisiae*. *Mol Cell Proteomics,* 17**,** 2309-2323.

Van Damme, P., Lasa, M., Polevoda, B., Gazquez, C., Elosegui-Artola, A., Kim, D. S., De Juan-Pardo, E., Demeyer, K., Hole, K., Larrea, E. et al. (2012). N-terminal acetylome analyses and functional insights of the N-terminal acetyltransferase NatB. Proc Natl Acad Sci U S A 109, 12449-54.

Vembar, S. S., Macpherson, C. R., Sismeiro, O., Coppee, J. Y. & Scherf, A. 2015. The PfAlba1 RNA-binding protein is an important regulator of translational timing in *Plasmodium falciparum* blood stages. *Genome Biol,* 16**,** 212.

Vincke, I. H. & Lips, M. 1948. A new plasmodium from a wild Congo rodent *Plasmodium berghei* n. sp. *Ann Soc Belg Med Trop (1920),* 28**,** 97-104.

Vizcaíno, J. A., Côté, R. G., Csordas, A., Dianes, J. A., Fabregat, A., Foster, J. M., Griss, J., Alpi, E., Birim, M., Contell, J., O'kelly, G., Schoenegger, A., Ovelleiro, D., Pérez-Riverol, Y., Reisinger, F., Ríos, D., Wang, R. & Hermjakob, H. 2013. The PRoteomics IDEntifications (PRIDE) database and associated tools: status in 2013. *Nucleic Acids Res,* 41**,** D1063-9.

Volkmann, K., Pfander, C., Burstroem, C., Ahras, M., Goulding, D., Rayner, J. C., Frischknecht, F., Billker, O. & Brochet, M. 2012. The alveolin IMC1h is required for normal ookinete and sporozoite motility behaviour and host colonisation in Plasmodium berghei. *PLoS One,* 7**,** e41409.

Wieczorek, S., Combes, F., Lazar, C., Giai Gianetto, Q., Gatto, L., Dorffer, A., Hesse, A. M., Coute, Y., Ferro, M., Bruley, C. & Burger, T. 2017. DAPAR & ProStaR: software to perform statistical analyses in quantitative discovery proteomics. *Bioinformatics,* 33**,** 135-136.

Xue, B., Jeffers, V., Sullivan, W. J. & Uversky, V. N. 2013. Protein intrinsic disorder in the acetylome of intracellular and extracellular *Toxoplasma gondii*. *Mol Biosyst,* 9**,** 645-57.

Zhang, M., Wang, C., Otto, T. D., Oberstaller, J., Liao, X., Adapa, S. R., Udenze, K., Bronner, I. F., Casandra, D., Mayho, M., Brown, J., Li, S., Swanson, J., Rayner, J. C., Jiang, R. H. Y. & Adams, J. H. 2018. Uncovering the essential genes of the human malaria parasite *Plasmodium falciparum* by saturation mutagenesis. *Science,* 360.

Figures

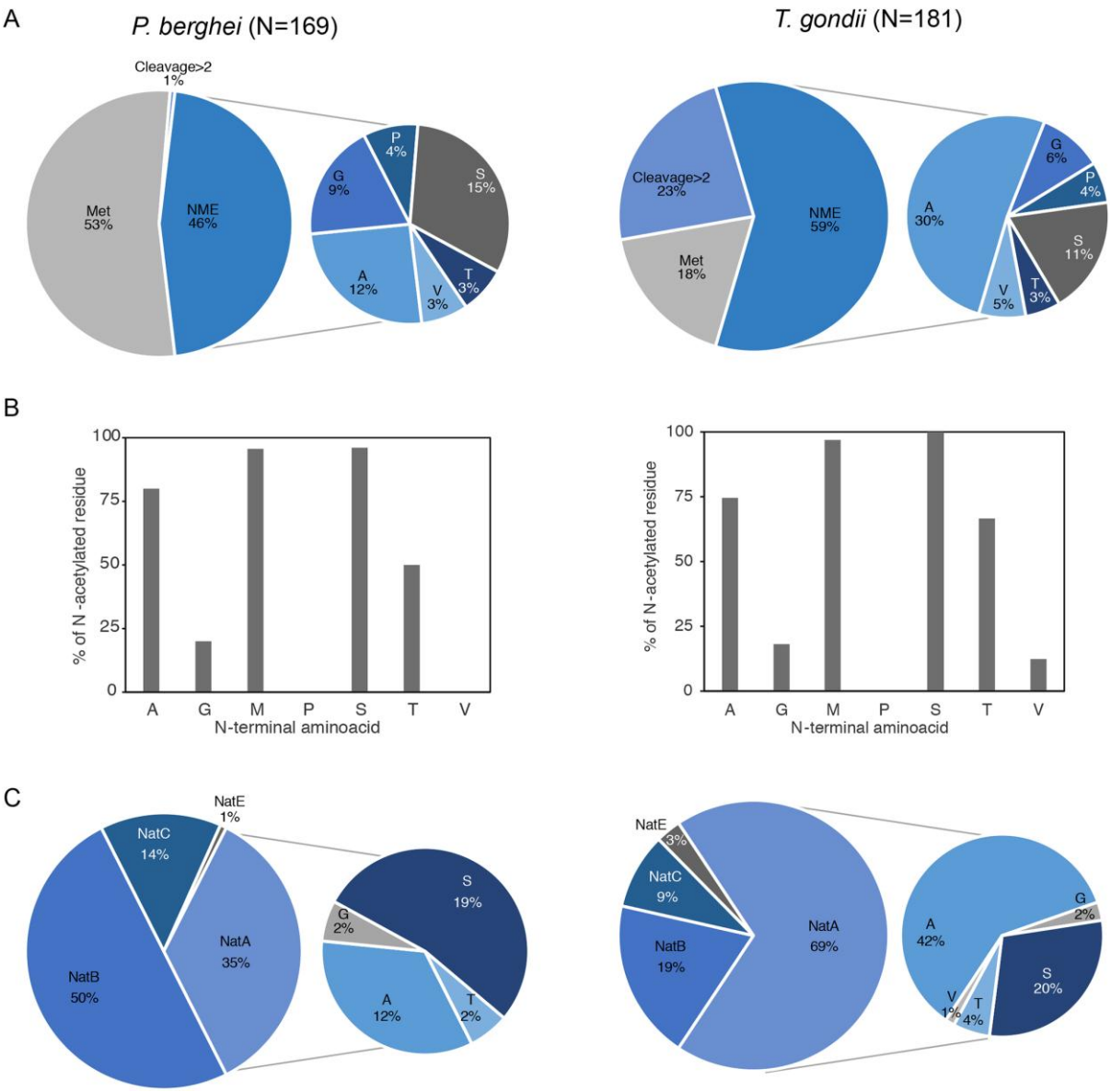

Figure 1 Distinct N-termini acetylation of *T. gondii* and *P. berghei* proteins

A) Summary of N-terminal Methionine Excision (NME) in *P. berghei* and *T. gondii*. B) Frequency of the retrieved N-terminal acetylated peptides analyzed according the nature of the N-terminal residue in both *P. berghei* and *T. gondii*. C) Overview of NAT substrate specificities. The number of N-terminal acetylated substrates with each of the major active NATs is displayed in a pie chart according to the classic Nat-type substrate distribution available.

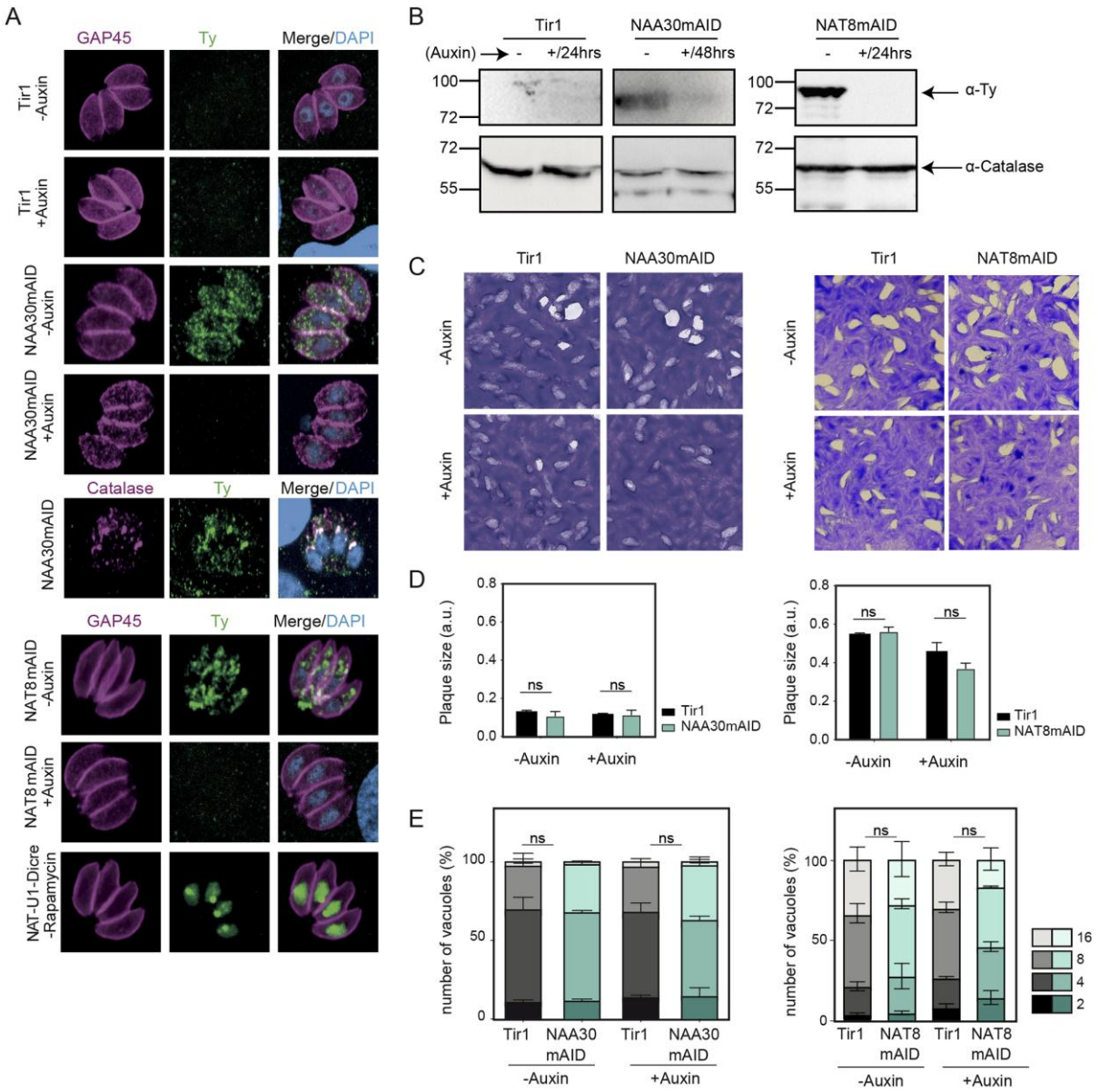

Figure 2 Putative GNAT acetyltransferases localize to the ER and nucleo-cytosol compartments of *T. gondii*

A) IFAs carried out using α-Ty antibodies and parasite periphery marker GAP45 on endogenously C-term tagged NAA30mAID-Ty, NAT8mAID-Ty parasites and control (Tir strain) under +/- Auxin conditions. NAA30mAID-Ty localize to the cytosol and partially colocalizes with a cytosolic protein, IFA conducted with α-catalase antibodies. NAT8mAID-Ty exhibits ER-like localization and NATU1-Dicre-Ty localizes to the nucleus (Magenta- GAP45; green Ty-tag). Scale bar 5µm. B) Immunoblots showing migration of TgNAT8 and TgNAA30 proteins between 70 and 100 kDa. Positive regulation of proteins indicated by loss of α-Ty signal upon addition of protein degradation inducer auxin for +24hours, Catalase was used a

positive control. C and D) Plaque assays of NAA30mAID-Ty and NAT8mAID-Ty parasites compared to control 7 days post infection of confluent human foreskin fibroblasts treated +/- Auxin. No impact on lytic cycle is observed confirmed by plaque size quantification compared to controls. Results are means of plaque areas ±SD of 3 independent experiments. Unpaired statistical significance applied * $p < 0.05$ values (Table S7). E) Intracellular growth of NAA30mAID-Ty and NAT8mAID-Ty. HFFs were infected with parasites and controls under +/- Auxin treatment and examined 24 hours post infection. Number of parasites per vacuole enumerated and shown as a percentage. A defect in replication observed in NAT8mAID-Ty parasites. Results are means ±SD of 3 independent experiments. Unpaired statistical significance applied * $p < 0.05$ values (Table S7).

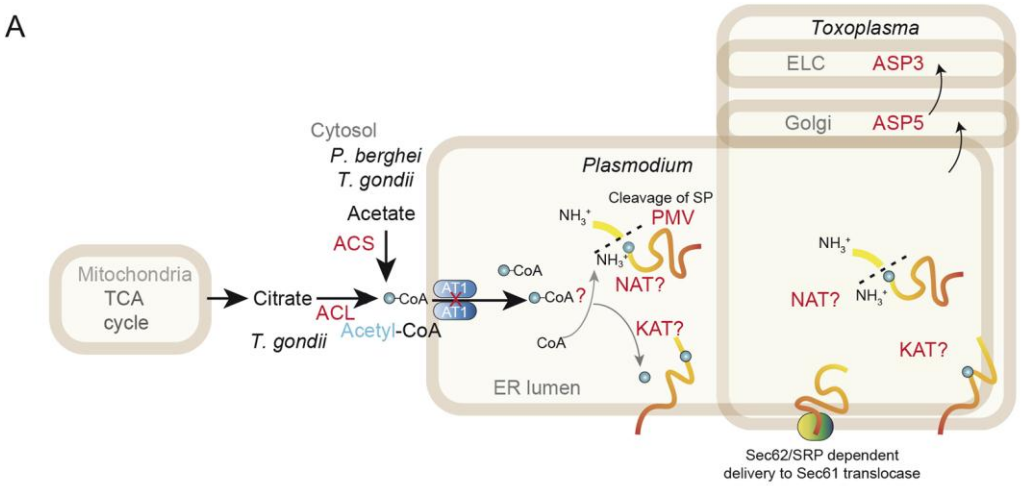

B

Gene name	Organism	Gene ID	Localisation	Fitness	Bradyzoites	Merozoites	Gametes	Oocyst	Coccidia	Haemosporidia	Piroplasmida	Cryptosporidia	Gregarina	Chromerida
Acetyl-coenzyme A transporter putative (AT1)	*P. berghei*	PBANKA_0519800		Slow										
	T. gondii	TGME49_215940	*ER	-0.07	-1.54	-1.40	-1.60	-1.40						

*: LOPIT/Publication
Slow (blood stage)

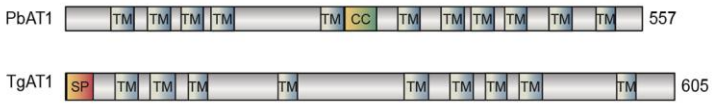

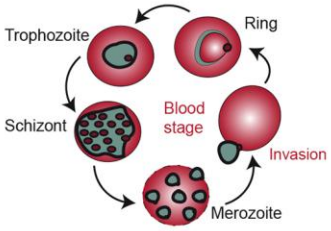

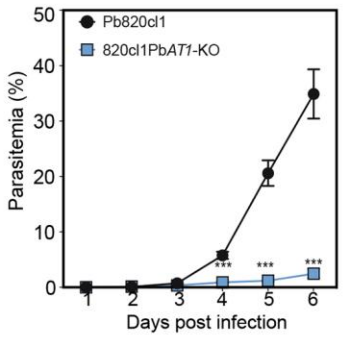

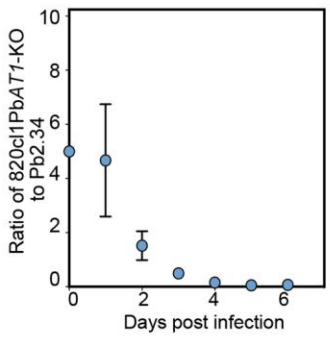

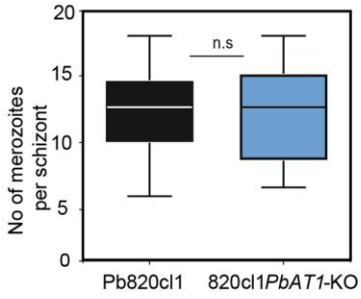

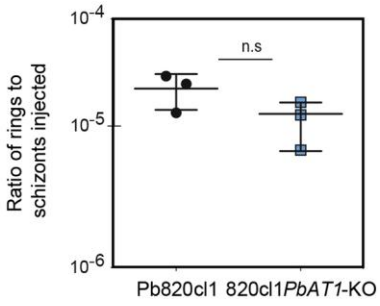

Figure 3 AT1 is a fitness determinant of *P.berghei* erythrocytic forms

A) Schematic illustration of acetyl-CoA synthesis in the cytosol of *T. gondii* and *P. berghei* by acetyl-CoA synthetase (ACS) and ATP citrate lyase (ACL) enzymes. Presence of AT1 on ER membrane and presumed role of AT1 in import of acetyl-CoA into ER lumen. Cleavage of peptides by Plasmodium Plasmepsin V (PMV) enzyme and acetylation by unknown N-acetyltransferases and K-acetyltransferases (NAT8) in the ER lumen. Aspartyl protease 5 (ASP5) and 3 (ASP3) cleave proteins in Golgi and endosomal like compartment respectively in *T. gondii*. B) Summary of conservation of *T. gondii* and *P. berghei AT1* gene in the Apicomplexa phylum based on BLAST search on VEuPathDB, expression of mRNAs at different stages of *T. gondii* lifecycle compared to tachyzoite stage, prediction of contribution to fitness for *T. gondii* based on genome wide CRISPR fitness screen (Sidik et al., 2016) and for *P. berghei* based on genome wide knock out screen (Bushell et al., 2017), localization of AT1 in *T. gondii* based on hyperplexed localisation of organelle proteins by isotope tagging (Barylyuk et al., 2020) . C) Graphic of PbAT1 and TgAT1 proteins, indicating amino acid length and putative domains, transmembrane domain TM, signal peptide SP, coiled coiled domain CC. D) Illustration of the steps in *Plasmodium* blood stage cycle. E) Marked low parasitemia in mice infected with 820cl1Pb*AT1*-KO parasites compared to wildtype measured by flow cytometry and presented as percentage parasitemia. N=5 per group. F) 820cl1Pb*AT1*-KO are out grown by wildtype parasites *in vivo* during parasite growth competition assessment by flow cytometry in 5:1 ratio of ko:wildtype. N=5 per group (Table S7). G) Comparable number of merozoites per schizont in wildtype and 820cl1Pb*AT1*-KO parasites counted from purified schizonts indicating normal development during the blood stage cycle. 100 schizonts counted per experiment, Box and whisker plots with minimum and maximum values, (n=3) (tBALE S7). H) Fewer rings detected post infection of mice with equal number wildtype and 820cl1Pb*AT1*-KO schizonts, n=3, plot is of means areas ±SD. Paired t test of statistical significance applied * $p < 0.05$ values (Table S7).

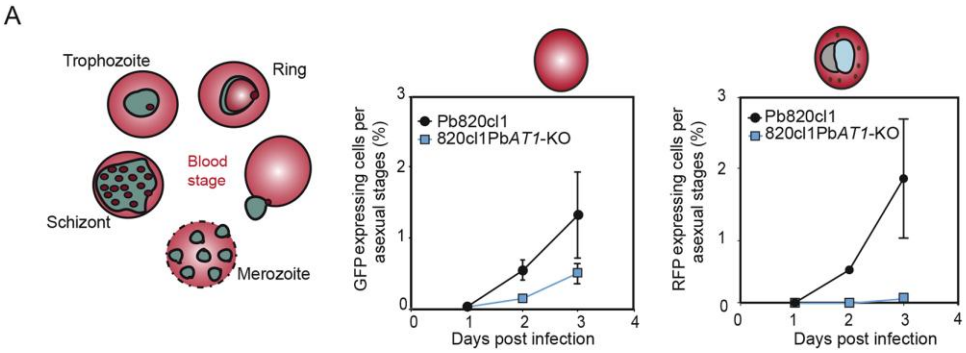

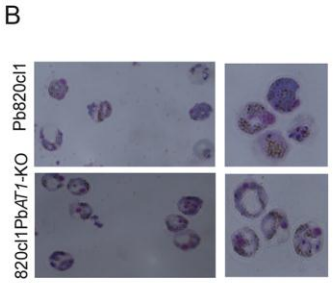

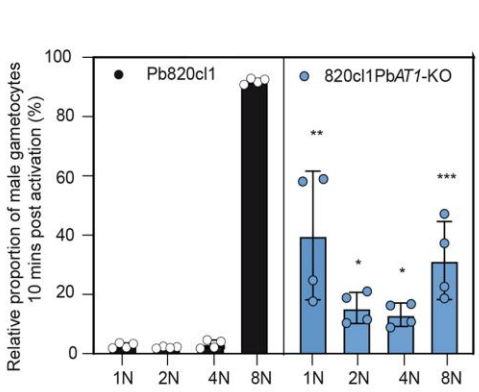

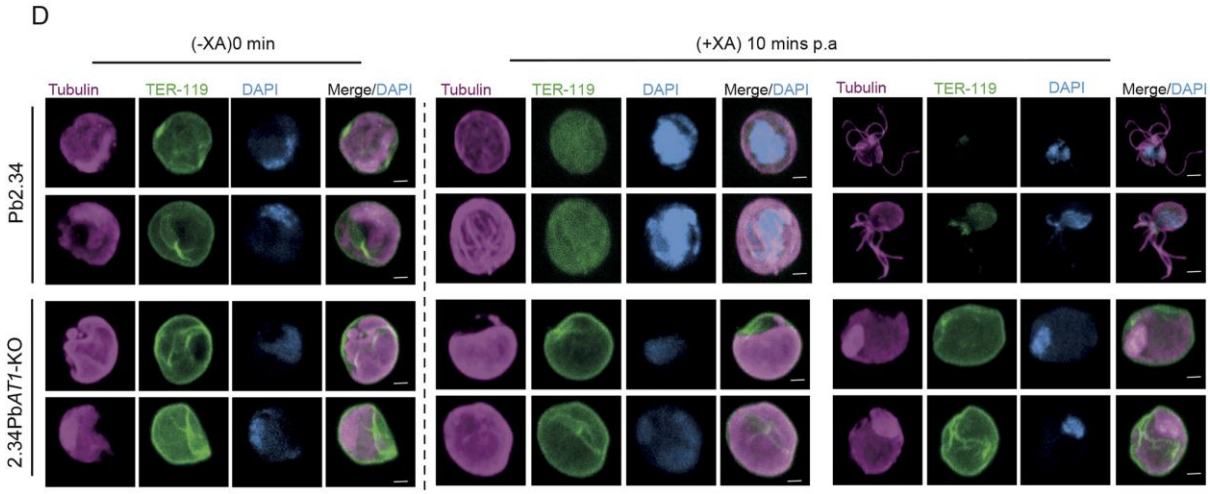

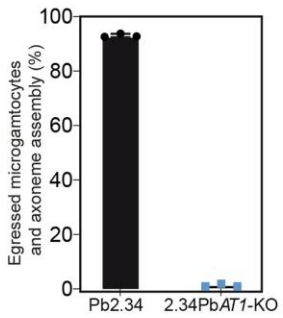

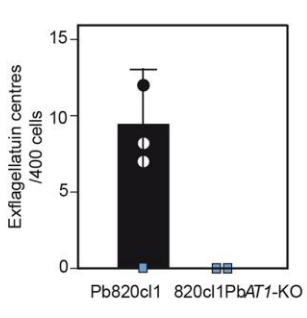

Figure 4 Impaired gametocytogenesis and gametogenesis in absence of *PbAT1.*

A) Flow cytometry measurements indicate fewer male microgametocytes (GFP) and no female macrogametocytes (RFP) detected in 820cl1Pb*AT1*-KO compared to wildtype parasites. Plot is percentage of cells expressing GFP or RFP per asexual forms, (n=4), means areas ±SD (Table S7). B) Representative image of Giemsa-stained blood films of purified gametocytes show 820cl1Pb*AT1*-KO male gametocytes appearing hollow compared to controls. C) Defective gametogenesis of male microgametocytes in 2.34Pb*AT1*-KO examined by IFA at 0 minutes -XA and 10 minutes +XA; (tubulin -magenta), egress from RBCs (TER-119, erythrocyte membrane marker-green) and DNA replication (DAPI) indicate absence of DNA replication, egress from erythrocytes and axoneme formation 10 minutes post XA activation. Inset representative images: IFA of WT 2.34Pb*AT1*-KO. Scale bar 2µm. D) Plot showing impaired gametogony, quantification of microgametocytes in 2.34Pb*AT1*-KO displaying axoneme assembly and egress from RBCs compared to wildtype parasites. N=3, plot is of means areas ±SD (Table S7). E) 820cl1Pb*AT1*-KO do not form exflagellation centers measured as motile active gametocytes 15 minutes post XA-activation. N=3, plot is of means ±SD (Table S7).

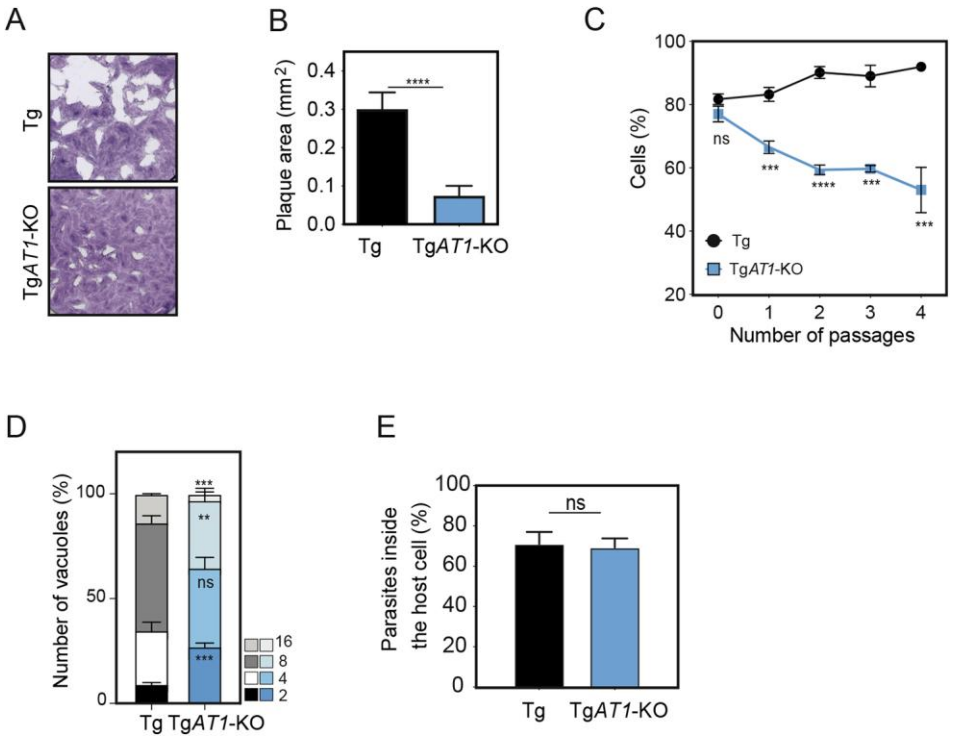

Figure 5 AT1 is a fitness conferring in *T. gondii* tachyzoite forms

A) Plaque assay of Tg*AT1*-KO parasites and control (Tg) 7 days post infection on confluent HFFs show severe impact on lytic cycle in Tg*AT1-KO* parasites, inset representative image of 3 independent experiments. B) Plaque size quantification of Tg*AT1*-KO compared to control (Tg) show significantly smaller lytic plaques formed by Tg*AT1*-KO. Results are means of plaque areas ±SD of 3 independent experiments. Unpaired statistical significance applied * $p < 0.05$ values (Table S7). C) Flow cytometry assessment of parasite growth in a competition assay of Tg*AT1*-KO with RHGFP parasites as an internal control over 4 consecutive lytic cycles in HFFs validates the significant defect in development (Table S7). D) Intracellular growth assay, HFFs were infected with Tg*AT1*-KO parasites and controls. IFAs were performed using GAP45 antibodies at 24 hours and number of parasites per vacuole enumerated and shown as a percentage. N=3, plot is of means ±SD (Table S7). Slower intracellular growth of Tg*AT1*-KO parasites compared to wildtype (Tg) is observed. E) Normal ability of Tg*AT1*-KO parasites to invade HFFs. Results are means ±SD of 3 independent experiments. Unpaired statistical significance applied * $p < 0.05$ values (Table S7).

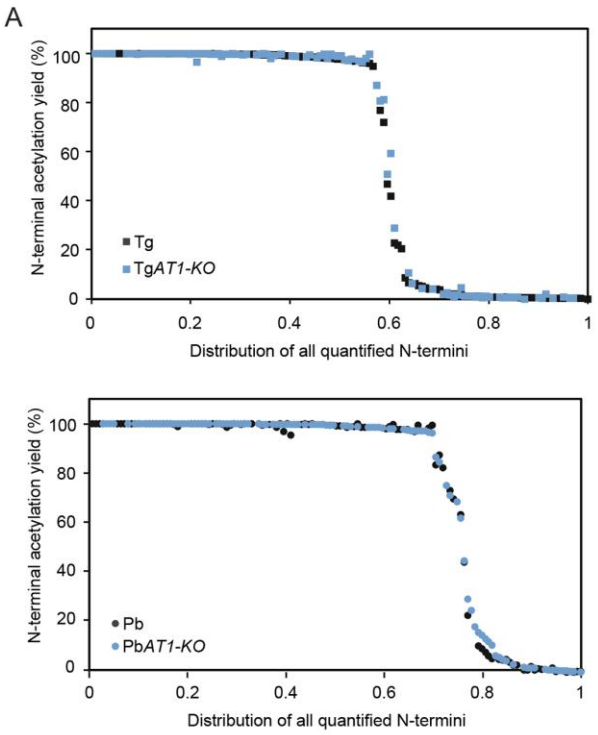

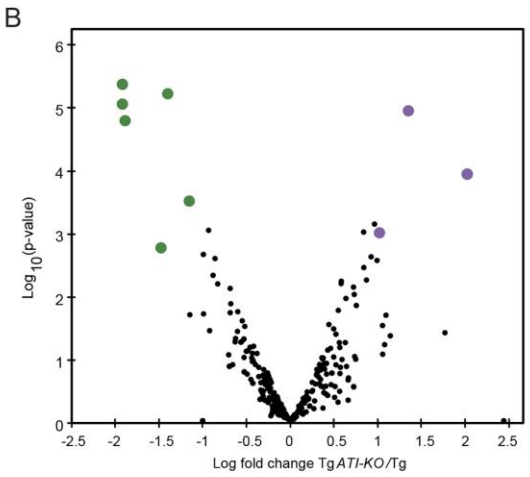

C

Gene name	Gene ID	Fitness	logFC (KO/WT)	Localisation (LOPIT)	Bradyzoites	Merozoites	Gametes	Oocyts
ribosomal protein RPS6 (RPS6)	TGME49_210690	-4.58	2.01	40S ribosome	0.6	3.0	1.9	2.3
phosphofructokinase (PFKII)	TGME49_226960	-5.19	1.35	Cytosol	-1.7	1.6	1.7	2.0
dehydrogenase E1 component family protein	TGME49_239490	-1.89	1.02	Mitochondrion - soluble	-1.1	2.1	3.4	2.7
dense granule protein GRA2 (GRA2)	TGME49_227620	2.47	-1.91	Dense granules	-0.1	-582.5	-3052.9	-3052.9
AP2 domain transcription factor (AP2X-7)	TGME49_214840	-3.39	-1.40	nucleus - chromatin	-1.2	-4.5	-4.1	-3.5
trypsin domain-containing protein	TGME49_262920	0.56	-1.47	Rhoptries	0.1	-4.8	-8.7	-6.0
hypothetical protein	TGME49_216060	0.12	-1.15	Nucleus - chromatin	-1.3	-2.3	-3.0	-2.2
hypothetical protein	TGME49_271740	0.36	-1.88	Nucleus - non-chromatin	-1.2	-3.0	-3.2	-2.8
hypothetical protein	TGME49_212220	-4.91	-1.91	Golgi	-0.3	-1.1	1.1	1.1

Figure 6 Lysine and N-terminal acetylome remain globally unalterated in both RHAT1-KO and PbAT1-KO

A) Comparison of NTA yield of retrieved N-termini of proteins in Tg*AT1*-KO and PbAT1-KO with corresponding WT (Tg and Pb, respectively). B) Comparative depiction of acetylation sites of Tg*AT1*-KO parasites and RH using Volcano plot. Statistically significant differences are determined as indicated in the materials and methods. In black, unchanged acetylation sites, in red hyperacetylated and in green hypoacetylated (> 2-fold, n=3). C) Summary of proteins with hyperacetylated and hypoacetylated sites indicating their hyperLOPIT predicted localization (Barylyuk et al., 2020), CRISPR Cas9 fitness prediction (colour gradient; blue dispensable, red essential)(Sidik et al., 2016) and mRNA expression at different stages compared to tachyzoite.

A

	Pb-WT (2 replicates)	PbAT1-KO (2 replicates)	Total
Identified N-termini	403	459	862
Non-redundant proteoforms	169	188	229
Quantified N-termini	101	105	132
Full acetylation (NTA > 95%)	72	76	-
Partial acetylation	11	13	-
No acetylation (NTA < 5%)	18	16	-
+NME (pos. 2)	45	41	52
Full acetylation (NTA > 95%)	24	22	-
Partial acetylation	7	8	-
No acetylation (NTA < 5%)	14	11	-
-NME (pos. 1)	55	62	78
Full acetylation (NTA > 95%)	48	54	-
Partial acetylation	4	5	-
No acetylation (NTA < 5%)	3	3	-

	RH-WT (3 replicates)	RH-AT1-KO (3 replicates)	Total
Identified N-termini	793	706	1499
Non-redundant proteoforms	181	143	200
Quantified N-termini	118	101	140
Full acetylation (NTA > 95%)	66	63	-
Partial acetylation	13	8	-
No acetylation (NTA < 5%)	39	30	-
+NME (pos. 2)	68	61	76
Full acetylation (NTA > 95%)	37	38	-
Partial acetylation	8	7	-
No acetylation (NTA < 5%)	23	16	-
iMet (pos. 1)	20	15	25
Full acetylation (NTA > 95%)	16	13	-
Partial acetylation	2	0	-
No acetylation (NTA < 5%)	2	2	-
Processed (pos. > 2)	30	25	39
Full acetylation (NTA > 95%)	13	12	-
Partial acetylation	3	1	-
No acetylation (NTA < 5%)	14	12	-

B

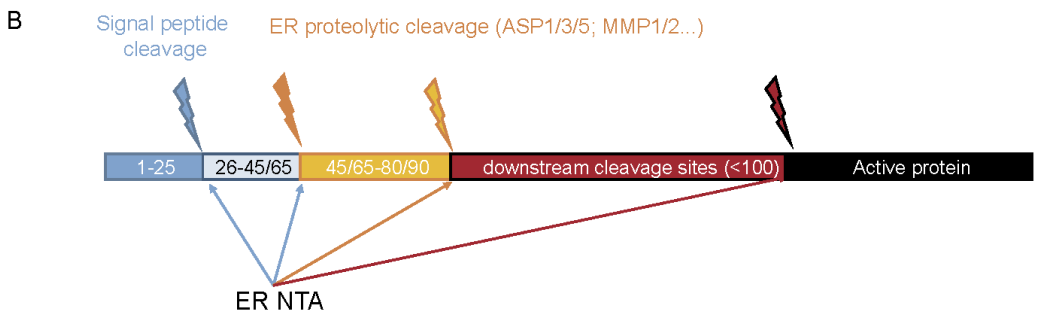

Fig. S1. Model for ER NTA in *T. gondii*

A) Summary of the NTA status and NME positioning of proteins in *P. berghei* and *T. gondii.* B) ER-NTA plausibly involves large spectrum Nat activity at the Signal peptide cleavage site, at the ER proteolytic cleavage site and within 100 amino acids downstream of cleavage.

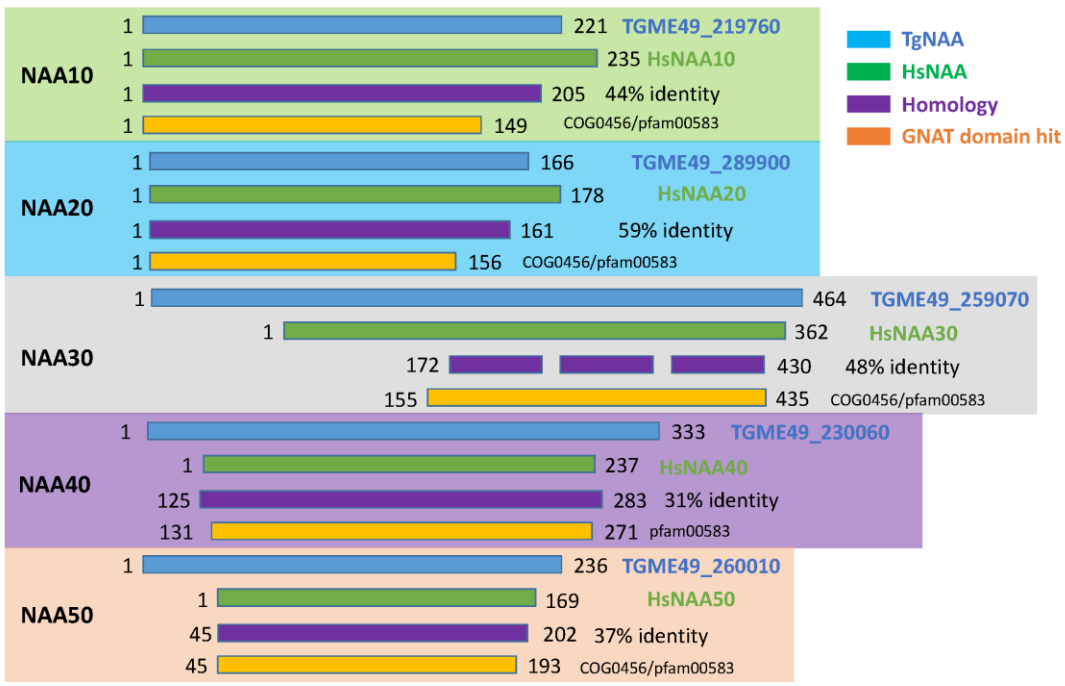

Fig. S2. Domains of candidates encoding the catalytic domains of Nat catalytic subunits in *T. gondii*.

Human catalytic subunits of NatA-E (ie NAA10-20-30-40-50) were used to challenge and identify the best matches in T*. gondii* using PSI-BLAST at NCBI. The identified sequences from the TGME ecotypes (one per subunits, blue) are indicates together with their alignment with the human counterpart (green), the homology regions (purple) and the identity percentage. The most significant structural domain hits (orange) are specified. They all correspond to the GNAT family N-acetyltransferase (domain architecture ID 11418877).

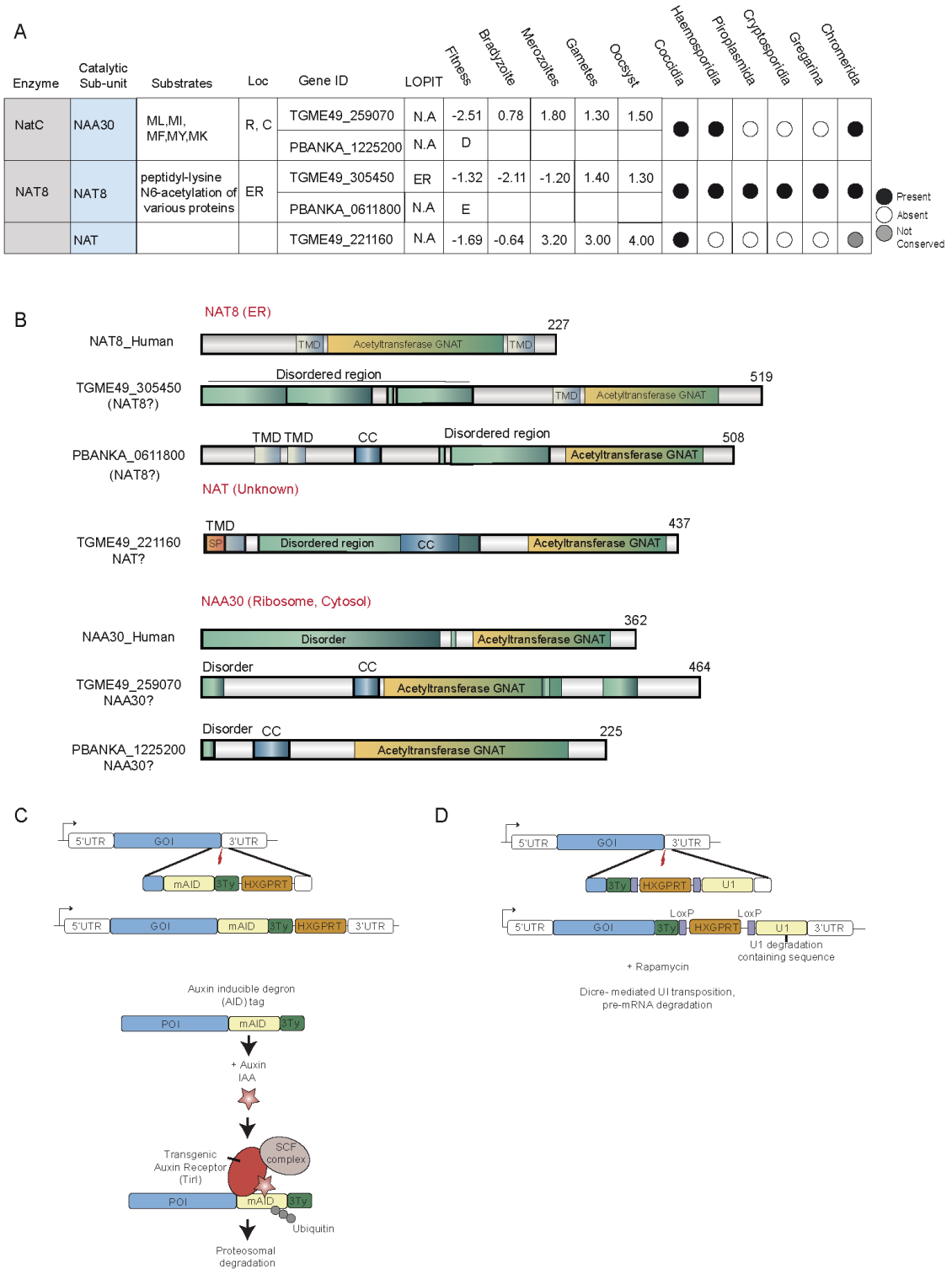

Fig. S3. Characterization of putative TgGNAT acetyltransferases

A) Summary of the key characteristics of the three targeted putative GNAT acetyltransferases in *T. gondii*. Conservation based on BLAST search on VEuPathDB, expression of mRNAs at different stages of *T. gondii* lifecycle compared to tachyzoite stage, prediction of contribution to fitness for *T. gondii* based on genome wide CRISPR fitness screen (Sidik et al., 2016), localization in *T. gondii* based on hyperplexed localisation of organelle proteins by isotope tagging (Barylyuk et al., 2020). B) Schematic illustration of the putative, TgNAT8, TgNAT and TgNAA30 proteins together with existing human and P. berghei homologues. Positioning of the putative transmembrane domain TMD, coil coil domain CC, signal peptide SP and the catalytic acetyltransferase domain are indicated. Protein down regulation strategies by C-term tagging of gene of interest with C) the Auxin inducible degron followed by protein degradation upon treatment with Auxin (IAA) D) DiCre mediated insertion of U1 recognition sites and recruitment of U1 machinery and pre-mRNA degradation upon treatment with Rapamycin.

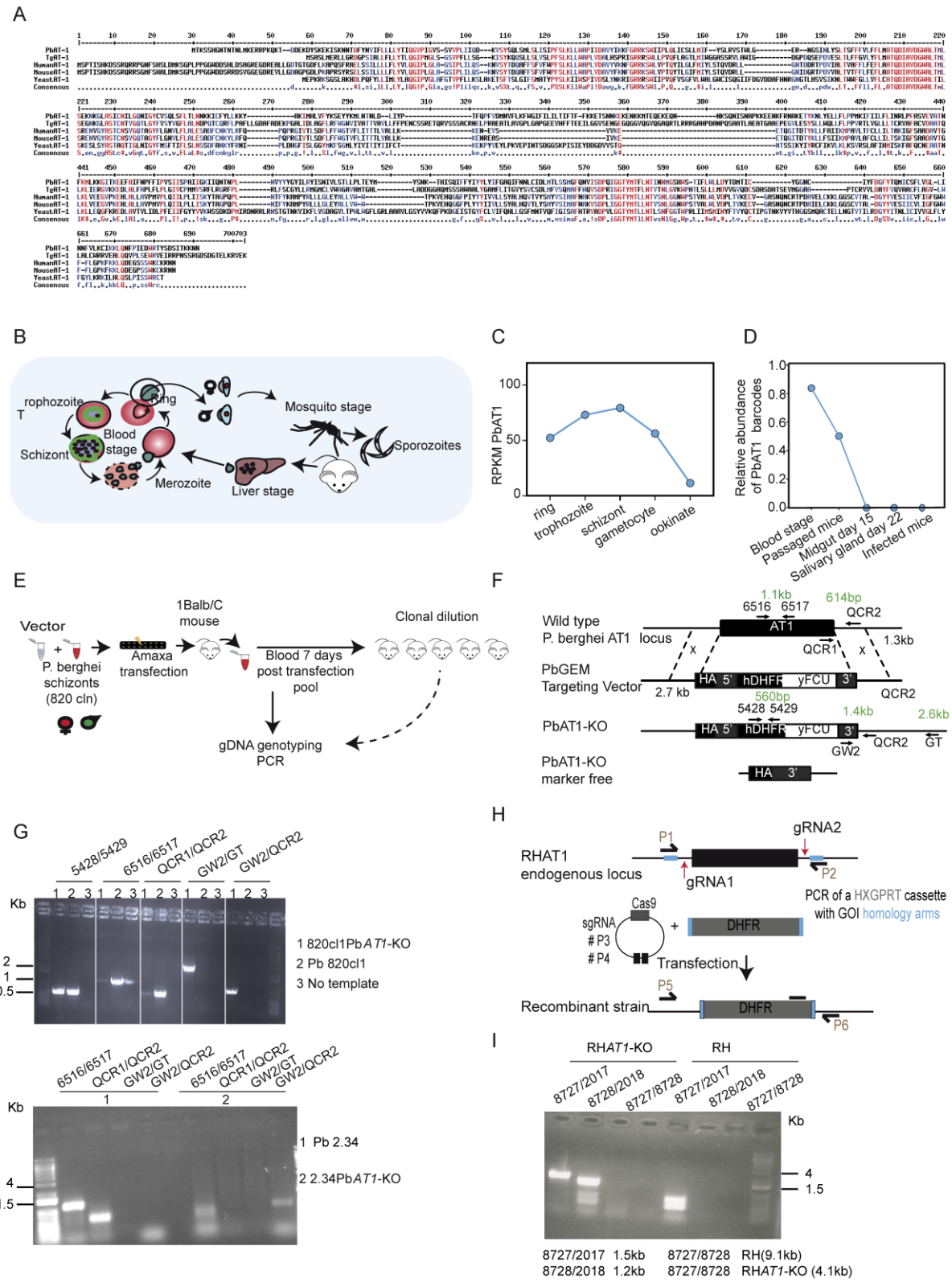

Fig. S4. Genome editing strategy to obtain Pb*AT1*-KO and Tg*AT1*-KO strains A) Multiple sequence alignment in MultAlin of AT1 sequences from *P. berghei* PBANKA_0519800, *T. gondii* TGME49_215940, *Mus musculus* Q99J27, and *Homo sapiens* O00400 and *Saccharomyces cerevisiae* P38318. Residues in red are highly

conserved, blue weakly conserved and dot in consensus denote no conservation. B) Schematic illustration of the complete life cycle of rodent *Plasmodium*. C) mRNA expression of PbAT1 during different stages of the life cycle, data extracted from (Caldelari et al., 2019). D) Detection of gene specific barcodes predicts essentiality of *PbAT1* for development in the mosquito, data extracted from (Stanway et al., 2019). E) Illustration of steps taken to obtain Pb*AT1*-KO including transfection of knock out vector in schizonts, infection of transfected schizonts and clonal dilution in mice and PCR for genotyping. F) Pb*AT1* replacement in both 820m1cl1 and 234 parental strains by homologous recombination using PbGEM targeting vector containing drug selection marker. G) PCR on gDNA extracted from wildtype and Pb*AT1*-KO carried out with primers indicated, expected amplification product sizes indicated. Primers sequences listed in supplemental (Table S6). H) Tg*AT1*-KO knock out strategy using specific gRNAs and CRISPR-CAS9 and homologous recombination replacement by selectable marker. I) PCR on genomic DNA expected sizes indicated, primers sequences listed in supplemental (Table S6).

Table S3. Relationships between NTA and protein compartmentalization and associated function in Apicomplexa

The data compile the annotations of data available in Table S1 and S2 for each parasite (see Sheets 4 and 3, and columns E-H,P and D-G,S, for *P. berghei* and *T. gondii* respectively).

Parasite		***Plasmodium berghei***				***Toxoplasma gondii***			
Compartments	**Sub-category (function)**	Number	%	Number of N-acetylated	% N-acetylated	Number	%	Number of N-acetylated	% N-acetylated
Nucleus	DNA-binding	18	9%	13	72%	13	9%	9	69%
	Import	4	2%	3	75%	0	0%	0	-
	RNA maturation	20	10%	11	55%	8	5%	5	63%
Cytosol	Translation	34	18%	17	50%	27	18%	12	44%
	Proteostasis	33	17%	20	61%	20	14%	13	65%
	Energy metabolism	11	6%	5	45%	9	6%	5	56%
	General metabolism	12	6%	10	83%	11	8%	9	82%
	Redox	3	2%	1	33%	1	1%	0	0%
	Signaling	8	4%	3	38%	6	4%	4	67%
	Cytoskeleton	2	1%	1	50%	7	5%	6	86%
Secretory	Endoplasmic Reticulum	7	4%	4	57%	7	5%	7	100%
	Golgi & Post-Golgi	9	5%	2	22%	16	11%	8	50%
Mitochondria		3	2%	2	67%	11	8%	1	9%
Plasma membrane		26	14%	14	54%	9	6%	5	56%
Vacuole		1	1%	0	0%	1	1%	1	100%
Apicoplast		0	0%	0	-	0	0%	0	-
Total/average		191	100%	106	55%	146	100%	85	58%

Table S4. GNAT candidates in apicomplexans

GCN5-related N-acetyltransferases family - GNAT acetyltransferases							Gene information (T. gondii)			Essentiality	Transcriptomics (RNA Seq) FC vs. tachyzoites				Protein information			P.falciparum		P.berghei	
Common name	**Catalytic subunit/ Auxiliary subunits**	**Gene ID Human catalytic subunit**	**Substrates**	**Usual subcellular localisation**	**Conservation**	**Annotation**	**LOPIT**	**ID**	**Gene product**	**5 guides**	**Bradyzoites**	**Merozoites**	**Gametes**	**Oocyts**	**# TM domains**	**Molecular weight (kDa)**	**Signal peptide**	**Gene ID**	**Essentiality**	**Gene ID**	**Essentiality**
NatA	NAA10	HGNC:18704	Protein N-termini starting with A,S,T,V,C,G	Ribosome, Cytosol, Nucleus	Yeast, Plants, Metazoa	NAA10	Outlier	TGME49_219760	N-acetyltransferase family protein	-4,19	-0,13	1,10	1,20	1,40	n/a	24,64	n/a	PF3D7_1003300	Essential	PBANKA_1201700	n/a
	NAA15					NAA15		TGME49_223710										PF3D7_1244100.1			
	HYPK				Not in some fungi	HYPK		No match										No match			
NatB	NAA20	HGNC:15908	Protein N-termini starting with MD,ME,MN,MQ	Ribosome, Cytosol	Yeast, Plants, Metazoa	NAA20	Not available	TGME49_289900	N-acetyltransferase family protein	-2,61	1,34	2,30	1,50	1,70	n/a	19,00	n/a	PF3D7_0109500	Essential	PBANKA_0204100	n/a
	NAA25					NAA25		TGME49_203750										No match			
NatC	NAA30	HGNC:19844	Protein N-termini starting with ML, MI, MF, MY, MK	Ribosome, Cytosol	Yeast, Plants, Metazoa	NAA30	Not available	TGME49_259070	acetyltransferase, GNAT family protein	-2,51	0,78	1,80	1,30	1,50	n/a	51,85	n/a	PF3D7_0805400	Dispensable	PBANKA_1225200	Dispensable
	NAA35					-		No match										No match			
	NAA38					-		No match										No match			
NatD	NAA40	HGNC:25845	Histones (H2A and H4) SGRGK	Ribosome, Cytosol, Nucleus	Yeast, Plants, Metazoa	NAA40	Nucleus-chromatin	TGME49_230060	acetyltransferase, GNAT family protein	-0,04	-0,03	1,10	1,30	1,10	n/a	37,24	n/a	PF3D7_1323300	Dispensable	PBANKA_1338500	n/a
NatE	NAA50 (within NatA)	HGNC:29533	Protein N-termini starting with MS, MT, MA, MV, ML, MI, MF, MY,	Ribosome, Cytosol,Nucleus	Yeast, Plants, Metazoa	NAA50	Cytosol	TGME49_260010	acetyltransferase, GNAT family protein	-2,26	-0,35	1,80	1,80	2,00	n/a	25,83	n/a	n/a	n/a	n/a	n/a
NatF	NAA60	HGNC:25875	Membrane protein N-termini starting with ML, MI, MY, MK	Golgi membrane	Yeast, Plants, Metazoa	NAA60	Not available	TGME49_260550	acetyltransferase, GNAT family protein	-1,34	0,82	-1,10	1,20	1,30	n/a	61,68	n/a	n/a	n/a	n/a	n/a
NatG	NAA70/NAA90	-	Chloroplast lumenal proteins starting with M,A,S,T	Plastid	Plants	-		No match										No match			
NatH	NAA80	HGNC:30252	Actin N-termini starting with DDD, EEE or DEE at positions 2 or 3 unmasked by acylaminoacid release	Cytosol	Metazoa, not identified in plants and fungi	NAA80		No match*										No match*			
NAT8	PMID:20392701 PMID:19011241 PMID:24556617	HGNC:18069	Internal lysine side chains of proteins	ER	Metazoa, not identified in plants and fungi	NAT8	ER	TGME49_305450	acetyltransferase, GNAT family protein	-1,32	-2,11	-1,20	1,40	1,30	1	56,86	n/a	PF3D7_1437000	Essential	PBANKA_0611800	Essential
ACAT1	PMID: 1979337	HGNC:93	Branched-chain amino acid catabolism	Mitochondria		Mitochondrial ACAT	Mitochondria	TGME49_301120	acetyl-CoA acetyltransferase	-3,63	-0,55	-1,90	-1,70	-1,50	n/a	43,89	n/a	PF3D7_1450900	Essential	PBANKA_1314600	Essential
ATAT1 alpha tubulin acetyltransferase 1		HGNC:21186		Cytoskeleton		ATAT	Not available	TGME49_319600	alpha-tubulin N-acetyltransferase, putative	-1,57	-1,80	-3,20	-1,20	-1,80	n/a	98,57	n/a	PF3D7_0924900	Dispensable	n/a	n/a
3-ketoacyl-CoA thiolase, peroxisomal (ACAA1)		HGNC:82		Peroxisome		ACAT	Not available	TGME49_273740	acetyl-CoA acyltransferase B, putative	1,33	2,61	10.2*	56.3*	31.9*	n/a	44,40	n/a	PF3D7_1450900	Essential	n/a	n/a
Homoserine O-acetyltransferase				Plastid		Apicoplast HTA, metX	Not available	TGME49_320730	homoserine O-acetyltransferase, putative	0,36	1,20	21.4*	123.9*	50.6*	n/a	48,02	NN Sum: 4, NN	n/a	n/a	n/a	n/a
?						TM domain (82-102), acetyltransferase (171-341)	Golgi	TGME49_219250	acetyltransferase, GNAT family protein	-0,09	-0,17	-1,30	-1,50	-1,10	1	89,52	n/a	n/a	n/a	n/a	n/a
?						?	Cytosol	TGME49_243600	acetyltransferase, GNAT family protein	1,41	1,03	1,10	2,30	1,90	n/a	55,43	n/a	PF3D7_0629000	Essential	PBANKA_1127600	n/a
?						?	Not available	TGME49_219180	acetyltransferase, GNAT family protein	1,46	0,81	-1,50	-2,90	-1,40	n/a	84,40	n/a	n/a	n/a	n/a	n/a
?							Not available	TGME49_221160	acetyltransferase, GNAT family protein	-1,69	-0,64	3,20	3,00	4,00	n/a	48,87	n/a	n/a	n/a	n/a	n/a

? (no match) or E value greater than 0.05

* the activity occurs in *T. gondii* as the acetylated version of actin was retrieved on E3. In *P. berghei* only the acetylated version on G2 was identified .

Table S6. Oligonucleotides used in this study

Primer name	Nr	Enzyme	Sequence (5'-3')	Resulting plasmid
TgAT-1.gRNA.1	8723	-	GTAAATGGGGATGTCAAGTTGCTCGGCTGCGACGTCTCTCGTTTTAGAGCTAGAAATAGC	CRISPR/Cas9
TgAT-1.gRNA.2	8724	-	GCTATTTCTAGCTCTAAAACACGAATCTCCACCCGCCACTCAACTTGACATCCCCATTTAC	CRISPR/Cas9
TgAT-1-DHFR.1	8725	-	TCGCTCTACTCTTCTCTCTCCGTTCGCGGCCGCTCTAGAACTA	TgAT-1-DHFR.1
TgAT1--DHFR.2	8726	-	GGAGAAAGTTCTCTCGACGCTCCATGCGGAAGATCCGATCTTGC	TgAT-1-DHFR.2
gRNA.1	4883	-	AACTTGACATCCCCATTTAC	CRISPR/Cas9
TgDHFR.1	2017	-	GTCACTTGTTGTGCCAGTTCTAC	Primer for screen
TgDHFR.2	2018	-	CTTGGGGGTCATCGCGACGACCAGAC	Primer for screen
TgAT-1.3	8727	-	GTGTCTCCTCTTTCTCTCGTTTCCTATG	Primer for screen
TgAT-1.4	8728	-	CTTCGTATTTCCTTTGCGTGGTGGC	Primer for screen (PbAT-1-KO)
QCR1	6354	-	TGGCGCGATTAGCAACACACA	Primer for screen (PbAT-1-KO)
QCR2	6355	-	AGGTTGAAAGAAAGGCACCA	Primer for screen (PbAT-1-KO)
GT	6515	-	GAACAGTCAACATCCCCACAATAGTAAAC	Primer for screen
GW2	6440	-	CTTTGGTGACAGATACTAC	Primer for screen PbAT-1-KO)
PbAT-1.1	6516	-	CAACCCAAGATATTGCAGTGGATG	Primer for screen
PbAT-1.2	6517	-	GTTCCGCCAATCTGTGGATCTG	Primer for screen
HDHFR.1	5428	-	GCCATGCATGCTGGTTCGCTAAACTGCATCG	Primer for screen
HDHFR.2	5429	-	CCGGCTTAGCTTAATCATTCTTCTCATATACTTCAAATTTGTAC	Primer for screen
TgNAT.gRNA.1	9988	-	GCAACGTCTCTGGTTGTAGCCGTTTTAGAGCTAGAAATAGC	CRISPR/Cas9
TgNAT.UI-Dicre.1	9991	-	TGCGTCGCTGGGCAGAGCAGGAAGAGGAAAGTGGCGCATGCATTGGAG	TgNAT-Dicre.1
TgNAT.UI-Dicre.2	9992	-	GCCTCGTTTCGCCAGGATTCTGGCCCAGACCAGGAAACAGCTATGACCATG	TgNAT-Dicre.2
TgNAA30.gRNA.1	9993	-	GCATCTAAATGTGTATAGATGTTTTAGAGCTAGAAATAGC	CRISPR/Cas9
TgNAA30.mAID.1	9994	-	AAGATTCTCAGCACATCCACTTGCTGGTGGGCTAGCAAGGGCTCGGG	TgNAA30-mAID.1
TgNAA30.mAID.2	9995	-	CAGGACACACTGACACACCGTTCTACATATATACGACTCACTATAGGG	TgNAA30-mAID.2
TgKAT.gRNA.1	9983	-	GTTCGCGCGTCGTGCCACAATGTTTTAGAGCTAGAAATAGC	CRISPR/Cas9
TgKAT.mAID.1	9984	-	GCGTTCAATCTTCCCTCCTCCATCCTCGACGCTAGCAAGGGCTCGGG	TgKAT-mAID.1
TgKAT.mAID.2	9985	-	AGAAGAGTTGAACAGAGCTGAGAGAAGGCGATACGACTCACTATAGGG	TgKAT-mAID.2

Table S7. Data used to generate figures and corresponding statistical analyses

	Egressed microgametocytes and aconeme assembly							
	Pb820cl1			**820cl1 PbAT11-KO**			**Unpaired t test**	**comment**
	Replicate 1	**Replicate 2**	**Replicate 3**	**Replicate 1**	**Replicate 2**	**Replicate 3**		
Activated	92.6	93.8	92.8	1.01	1.97	1.03	< 0.0001	****
Non activated	7.4	6.2	7.2	98.93	98.3	98.97	< 0.0001	****